

**An-Najah National University**  
**Faculty of Graduate Studies**

# **Pentavalent Ions Sorption on Bentonite Clay**

**By**  
**Sojoud Adnan Odeh**

**Supervisor**  
**Dr. Zeid Qamhieh**

**Co- Supervisor**  
**Dr. Khawla Qamhieh**

**This Thesis is Submitted in Partial Fulfillment of the Requirements for  
the Degree of Master of Physics, Faculty of Graduate Studies, An-  
Najah National University - Nablus, Palestine.**

**2015**

# Pentavalent Ions Sorption on Bentonite Clay

By  
Sojoud Adnan Odeh

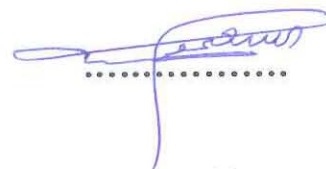
This thesis was defended successfully on 19/1/2015 and approved by:

## Defense Committee Members

## Signature

– Dr. Zeid Qamhieh

(Supervisor)



– Dr. Khawla Qamhieh

(Co- Supervisor)



– Prof. Mohammad Abu Samra

(External Examiner)



– Prof. Issam Abdelraziq

(Internal Examiner)



### III

## Dedication

To my parents (*Adnan & Obaida*), who are impossible to be thanked adequately for everything they have done. They are the best model for perfect parents. God bless them.

To my beloved husband (*Hasan*), who shares me all moments even by signing his existence with a smile. He also provides me with encouragement, motivation and support to overcome all difficulties to continue moving forward. He is truly a big grace to be in my life.

To the wonderful persons in my life; my uncles (*Zahran, Basim & Ghassan*) and my aunt (*Zuhdeia*).

To my kind sisters (*Fatima & Taqwa*) and brothers (*Moath, Obay & Huthaifa*), who always are there for me.

To my smart, cute baby (*Ali*). God bless him.

## **Acknowledgment**

All thanks to Almighty Allah, Most Gracious and Most Merciful who endows me with blessing, health, patience and knowledge to complete my thesis.

Special thanks to An-Najah National University for allowing me using its facilities and supports. I am really grateful to precious time, sincere efforts and constructive guidance granted to me by my supervisor **Dr. Zeid Qamhieh**. I am also thankful to my co-supervisor **Dr. Khawla Qamhieh** for her cooperation and valuable helping advice. Never forget my faculty members of physics department for their help and encouragement. Finally, especial thank to my relatives and friends for their moral support and cares.

## الإقرار

أنا الموقع أدناه مقدم الرسالة التي تحمل العنوان:

### Pentavalent Ions Sorption on Bentonite Clay

أقر بأن ما اشتملت عليه هذه الرسالة، إنما هي نتاج جهدي الخاص، باستثناء ما تمت الإشارة إليه حيثما ورد، و أن هذه الرسالة ككل، و أي جزء منها لم يقدم من قبل لنيل درجة علمية أو بحث علمي لدى أي مؤسسة تعليمية أو بحثية أخرى.

#### Declaration

The work provided in this thesis, unless otherwise referenced, is the researcher's own work, and has not been submitted elsewhere for any other degree or qualification.

Student's name:

اسم الطالب: سجاد عرنان عودة

Signature:

التوقيع: سجاد

Date:

التاريخ: 10 / 11 / 19

## Table of Contents

No.	Content	Page
	Dedication	III
	Acknowledgment	IV
	Declaration	V
	Table of Contents	VI
	List of Figures	VIII
	List of Symbols and Abbreviations	XIII
	Abstract	XIV
	<b>Chapter One: Introduction</b>	1
1.1	Solutions for Handling Waste Water and SKB Method	1
1.2	Literature Review	4
1.3	Objectives	7
	<b>Chapter Two: Theoretical Background</b>	9
2.1	Clay Minerals	9
2.2	Bentonite Clay Structure	11
2.3	Diffuse Double Layer	14
2.4	Spatial Distribution of Counterions	17
2.5	Sorption Process in Montmorillonite	20
2.5.1	Sorption Mechanisms	20
2.5.2	Distribution Coefficient Concept	23
2.5.3	Factors Affecting Sorption Process	24
	<b>Chapter Three: Model and Numerical Methodology</b>	25
3.1	Model System	25
3.2	Method	27
3.2.1	Markov Chain	28
3.2.2	Metropolis Algorithm	29
3.2.3	Grand Canonical Ensemble	31
3.2.3.1	Statistical Mechanical Basis	31
3.2.3.2	Monte Carlo Implementation	34
3.2.4	Periodic Boundary Conditions	35
3.2.5	Minimum Image Conventional Technique	36
3.2.6	Methodology	37
	<b>Chapter Four: Results and Discussion</b>	41
4.1	Fraction of Different Cations in EDL	42
4.2	Effect of Pentavalent Cations Concentration in the Two Bulk Solutions	45
4.3	Effect of Surface Charge Density	51
4.4	Effect of Temperature	58
4.5	Effect of Solution Ionic Strength	62
4.5.1	Effect of Divalent Ionic Strength	62

## VII

4.5.2	Effect of Monovalent Ionic Strength	69
	<b>Chapter Five: Conclusions</b>	76
	References	78
	المخلص	ب

VIII  
**List of Figures**

No.	Caption	Page
<b>Figure 1.1</b>	SKB method for final disposal of radioactive wastes. (a) The copper canister with iron insert, (b) the bentonite clay as a buffer and backfill material and (c) the crystalline bedrock. (www.quintessa.org).	3
<b>Figure 2.1</b>	Diagrammatic sketch illustrates (a) a single tetrahedron unit and (b) isometric view of tetrahedral sheet. (Grim, 1968).	10
<b>Figure 2.2</b>	Diagrammatic sketch illustrates (a) a single octahedron unit and (b) isometric view of octahedral sheet. (Grim, 1968).	10
<b>Figure 2.3</b>	Diagrammatic sketch of montmorillonite structure. (Grim, 1962).	12
<b>Figure 2.4</b>	(a) Helmholtz model which is identical to parallel plate capacitor. (b) The electrical potential of the aqueous solution is falling sharply. (Mitchell, 1993).	15
<b>Figure 2.5</b>	(a) Gouy-Champan model that has a diffuse layer. (b) The electrical potential of the solution is decreasing exponentially from the charged surface to the extended solution. (Mitchell, 1993).	16
<b>Figure 2.6</b>	(a) Stern Gouy-Champan model which forms of a compact layer of finite radius of cations known as Stern layer and a diffuse layer of anions and cations extending into the electrolyte solution. (b) The electrical potential decays with distance. (Mitchell, 1993).	17
<b>Figure 2.7</b>	Replaceability of exchangeable cations as $\text{Ca}^{2+}$ , $\text{Na}^+$ for $\text{Sr}^{2+}$ radionuclide and balancing the negative charge on the clay surface excess from isomorphic substitution of $\text{Al}^{3+}$ for $\text{Si}^{4+}$ , in tetrahedral, and $\text{Mg}^{2+}$ for $\text{Al}^{3+}$ , in octahedral, of bentonite minerals with $\text{Sr}^{2+}$ . (Poernomo, 2010).	21
<b>Figure 3.1</b>	Two infinite parallel walls of a uniform surface charge density a distance $h$ apart. The ions are treated as charged hard spheres and water is modeled as a dielectric continuum with a relative dielectric permittivity constant $\epsilon_r$ . (Segad <i>et al.</i> , 2010).	25
<b>Figure 3.2</b>	The procedure of accepting or rejecting the trial	31



	moves in Monte Carlo simulation using Metropolis algorithm. That is, if $\zeta_1$ is chosen, the attempt is accepted with probability of $\exp[-\beta \Delta u_{lh}]$ , while if $\zeta_2$ is chosen, the attempt is rejected. (Allen and Tildesley, 1987).	
<b>Figure 3.3</b>	A two-dimensional 2D periodic model. The central square is the original one and the duplicate squares are labeled as A, B, C ... etc. When particle 1 moves through the edge of the square, its images 1A, 1B ... etc also move through their corresponding edges. In 3D periodic system, the particle is free to leave the box through six cubic faces. (Allen and Tildesley, 1987).	36
<b>Figure 3.4</b>	Minimum image conventional technique in two-dimensional system. The potential energy containing particle 1 is the addition of the interaction pairs between particles of 1, 2, 4E, 3E and 5C. (Allen and Tildesley, 1987).	37
<b>Figure 4.1</b>	Fraction of different counterions in the water slit as a function of pentavalent cations concentration in the bulk solutions. The slit is in equilibrium with a bulk including: a) 1 mM NaCl, 4 mM CaCl <sub>2</sub> (ground water), b) 100 mM NaCl, 10 mM CaCl <sub>2</sub> (sea water) and varied amount of pentavalent cations. The surface charge density has been varied as pointed in the graphs. The slit width is 3 nm.	42
<b>Figure 4.2</b>	Average electrical double layer concentration of the pentavalent cations as a function of their concentrations in the bulk. The bulk also includes a) 1 mM NaCl, 4 mM CaCl <sub>2</sub> b) 100 mM NaCl, 10 mM CaCl <sub>2</sub> . The surface charge density has been varied as pointed in the graphs. The slit width is 3 nm.	46
<b>Figure 4.3</b>	Counterion distribution as a function of distance $z$ outside the charged surface. Two different bulk systems are shown with a) 1 mM NaCl, 4 mM CaCl <sub>2</sub> b) 100 mM NaCl, 10 mM CaCl <sub>2</sub> and the concentration of pentavalent cations is increased from 0.00001 mM (dashed lines) to 0.001 mM (solid lines). The surface charge density is $-3 \text{ e/nm}^2$ and the slit width is 3 nm. Na <sup>+</sup> (red curves), Ca <sup>2+</sup> (green curves) and M <sup>5+</sup> (blue curves).	47

<b>Figure 4.4</b>	Pentavalent cations distribution as a function of distance $z$ outside the charged surface. Two different bulk systems are shown with a) 1 mM NaCl, 4 mM CaCl <sub>2</sub> b) 100 mM NaCl, 10 mM CaCl <sub>2</sub> and different values of pentavalent cations concentration as pointed in the graphs. The slit width is 3 nm and the surface charge density is a) $-0.7 \text{ e/nm}^2$ b) $-2 \text{ e/nm}^2$ .	49
<b>Figure 4.5</b>	The retention coefficient calculated from the curves in Figure 4.2.	49
<b>Figure 4.6</b>	Average electrical double layer concentration of pentavalent cations as a function of surface charge density of the two separated walls. The bulk concentration of pentavalent cations has been varied as pointed in the graphs. The bulk also includes a) 1 mM NaCl, 4 mM CaCl <sub>2</sub> b) 100 mM NaCl, 10 mM CaCl <sub>2</sub> .	51
<b>Figure 4.7</b>	Average electrical double layer concentration of a) trivalent ( $M^{3+}$ ) and b) tetravalent ( $M^{4+}$ ) cations as a function of surface charge density. The bulk contains 100 mM NaCl, 10 mM CaCl <sub>2</sub> and varied amount of the multivalent species	53
<b>Figure 4.8</b>	Counterion distribution as a function of distance $z$ outside the charged surface. The bulk solution contains 100 mM NaCl, 10 mM CaCl <sub>2</sub> and 0.0001 mM of pentavalent cations. The surface charge density has been varied; green curves = $-2 \text{ e/nm}^2$ , red curves = $-3 \text{ e/nm}^2$ and blue curves = $-4 \text{ e/nm}^2$ . The slit width is 3 nm. Na <sup>+</sup> (solid lines), Ca <sup>2+</sup> (dashed lines) and M <sup>5+</sup> (dot-dashed lines).	54
<b>Figure 4.9</b>	The retention coefficient calculated from the curves in Figure 4.6.	55
<b>Figure 4.10</b>	Comparison of sorption data for Np(V) actinide on bentonite and montmorillonite from different studies. Data sources contain: (1) (Beall and Allard, 1981), (2) (Allard et al., 1984), (3) (Torstenfelt et al., 1988), (4) (Sakamoto et al., 1990), (5) (Triay et al., 1993), (6) (Ohe et al., 1993) and (7) (Kozai, 1994). (Turner et al., 1998).	56
<b>Figure 4.11</b>	Average electrical double layer concentration of the pentavalent cations as a function of temperature. The slit is in equilibrium with a bulk	59

	including a) 1 mM NaCl, 4 mM CaCl <sub>2</sub> b) 100 mM NaCl, 10 mM CaCl <sub>2</sub> . The surface charge density and the pentavalent cations concentration have been varied as pointed in the graphs. The slit width is 3 nm. The solid curves are linear fitting, while the dots are simulated results.	
<b>Figure 4.12</b>	The retention coefficient calculated from the data in Figure 4.11. The solid curves are linear fitting, while the dots are simulated results.	60
<b>Figure 4.13</b>	Pentavalent cations distribution as a function of distance $z$ outside the charged surface. The bulk solution contains 1 mM NaCl, 4 mM CaCl <sub>2</sub> and 0.1 mM of pentavalent cations. The temperature has been varied as pointed in the graph at surface charge density of $-0.7 \text{ e/nm}^2$ . The slit width is 3 nm.	61
<b>Figure 4.14</b>	Fraction of different counterions in the slit as a function of pentavalent cations concentration in the bulk solution. The surface charge density has been kept constant as pointed in the plots. But the bulk conditions have been varied; a) 1 mM NaCl, X mM CaCl <sub>2</sub> b) 100 mM NaCl, X mM CaCl <sub>2</sub> . The slit width is 3 nm. The values of X are obvious in the graphs.	63
<b>Figure 4.15</b>	Average electrical double layer concentration of pentavalent cations as a function of CaCl <sub>2</sub> concentration at surface charge densities of $-3$ and $-4 \text{ e/nm}^2$ . The bulk includes a) 1 mM NaCl, X mM CaCl <sub>2</sub> b) 100 mM NaCl, X mM CaCl <sub>2</sub> and 0.00001 mM of pentavalent cations. The solid curves are linear or exponential fitting, while the dots are simulated results.	65
<b>Figure 4.16</b>	The retention coefficient calculated from the data in Figure 4.15. The solid curves are linear or exponential fitting, while the dots are simulated results.	66
<b>Figure 4.17</b>	Counterion distribution as a function of distance $z$ outside the charged surface. Different bulk solutions are shown with 1 mM NaCl and varied amount of CaCl <sub>2</sub> concentration. The surface charge density is $-4 \text{ e/nm}^2$ and the pentavalent cations concentration is 0.00001 mM.	67

<b>Figure 4.18</b>	Average electrical double layer concentration of pentavalent cations as a function of their bulk concentration. The bulk conditions have been varied; a) 1 mM NaCl, X mM CaCl <sub>2</sub> b) 100 mM NaCl, X mM CaCl <sub>2</sub> at surface charge density of -3 and -4 e/nm <sup>2</sup> . The slit width is 3 nm.	68
<b>Figure 4.19</b>	The retention coefficient calculated from the curves in Figure 4.18.	69
<b>Figure 4.20</b>	Fraction of different counterions in the slit as a function of pentavalent cations concentration in the bulk solution. The surface charge density has been kept constant as pointed in the plots. While the bulk conditions have been varied; a) X mM NaCl, 4 mM CaCl <sub>2</sub> b) X mM NaCl, 10 mM CaCl <sub>2</sub> . The slit width is 3 nm. The values of X are obvious in the graphs.	70
<b>Figure 4.21</b>	Average electrical double layer concentration of pentavalent cations as a function of NaCl concentration at surface charge densities of -3 and -4 e/nm <sup>2</sup> . The bulk includes a) X mM NaCl, 4 mM CaCl <sub>2</sub> b) X mM NaCl, 10 mM CaCl <sub>2</sub> and 0.00001 mM of pentavalent cations. The solid curves are linear fitting, while the dots are simulated results.	72
<b>Figure 4.22</b>	The retention coefficient calculated from the data in Figure 4.21. The solid curves are linear fitting, while the dots are simulated results.	73
<b>Figure 4.23</b>	Counterion distribution as a function of distance z outside the charged surface. Two different bulk systems are shown with a) 400 mM NaCl, 4 mM CaCl <sub>2</sub> (solid lines) and 800 mM NaCl, 4 mM CaCl <sub>2</sub> (dashed lines) b) 200 mM NaCl, 10 mM CaCl <sub>2</sub> (solid lines) and 500 mM NaCl, 10 mM CaCl <sub>2</sub> (dashed lines). The slit width is 3 nm.	74
<b>Figure 4.24</b>	The retention coefficient of pentavalent cations as a function of a) NaCl b) CaCl <sub>2</sub> concentration at surface charge density of -3 e/nm <sup>2</sup> with 10 <sup>-5</sup> mM of M <sup>5+</sup> cations. The decreasing rate of the curves is indicated in the plots. The solid curves are linear fitting, while the dots are simulated results.	75

**List of Symbols and Abbreviations**

$c_B$	Concentration of a cation in the bulk solution
$\langle c_{EDL} \rangle$	Average electrical double layer concentration of a cation
DDL	Diffuse double layer
DLVO	Derjaguin – Landau – Verwey – Overbeek
EDL	Electrical Double Layer
GCMC	Grand Canonical Monte Carlo
$k_B$	Boltzmann constant
$k_d$	Distribution coefficient
mM	Millimolar
mV	Millivolt
$M^{5+}$	Cation with valency 5
P–B	Poisson-Boltzmann equation
SKB	Swedish Nuclear Fuel and Waste Management Company
$U(r)$	Potential at distance $r$
$V$	Volume
$v_i$	Valency of ion $i$
$z$	Distance from the charged wall
$Z$	Grand canonical partition function
$\alpha_{frac}$	Fraction
$\epsilon_0$	Vacuum permittivity
$\epsilon_r$	Relative dielectric permittivity
$\rho_{ch}$	Volume charge density
$\Phi$	Electrical potential opposite the charged surface
$\mu$	Chemical potential
$\Lambda$	Thermal de Broglie wavelength
$\zeta$	Random number
$\gamma$	Retention coefficient
$\sigma$	Surface charge density

XIV  
**Pentavalent Ions Sorption on Bentonite Clay**  
**By**  
**Sojoud Adnan Odeh**  
**Supervisor**  
**Dr. Zeid Qamhieh**  
**Co- Supervisor**  
**Dr. Khawla Qamhieh**

**Abstract**

Sorption of pentavalent radioactive pollutants from ground and sea water to bentonite clay was studied under various conditions using Monte Carlo simulation. The primitive model was used in which water of a certain dielectric permittivity constant is contained, and the ions are treated as charged hard spheres with the same diameter. Furthermore, the clay platelets were considered to be two parallel planer uniformly charged surfaces. Depending on a series of simulations in grand canonical ensemble, the average electrical double layer concentration and the retention coefficient of pentavalent cations were calculated as a function of pentavalent concentration in the aqueous solution, temperature of the whole system, surface charge density on the platelets and ionic strength of the solution.

The results of this study indicate that, the sorption behavior of pentavalent cations is strongly influenced by the previously mentioned parameters. In particular, the average electrical double layer concentration of pentavalent cations increases by increasing the bulk concentration of pentavalent pollutants and the surface charge density. This average concentration decreases by increasing the ionic strength. However, the retention

coefficient of pentavalent cations tends to increase by increasing the surface charge density whilst it becomes less by increasing the pentavalent concentration in the bulk and the ionic strength. Moreover, the average concentration and the retention coefficient of pentavalent cations decrease very slightly with increasing temperature. Besides, the results show that bentonites are suitable sorbents for recovery and sorption of pentavalent radioactive pollutants from different aqueous solutions.

# Chapter One

## Introduction

Contamination with radionuclides resulted from the widespread sources of radioactive wastes forms a critical threat to ground water. The leakage of radioactive metals to the ground water causes polluted waste water. Because of the harmful effects on human beings due to the toxicity of those metals even at low concentrations and their long half life times, the treatment of this serious problem is obviously of great concern as would be seen in the following section.

### 1.1 Solutions for Handling Waste Water and SKB Method

A number of different conventional techniques have been investigated for disposal and elimination of radioactive metals from waste water. These approaches include precipitation, solvent extraction and electrochemical treatment (Li *et al.*, 2009). Besides, aeration, oxidation and filtration method which is applied in Estonian ground water treatment (Lumiste *et al.*, 2012). Among all the proposed methods, sorption is the most popular one that is simply applied, effective and economic (Zhao *et al.*, 2011).

The term sorption relates to all processes in which the concentration of dissolved species increases at the interface between the aqueous phase and the solid surface (solid-solution interface). The sorption includes adsorption (when the element is attached on the surface by adhering) and absorption (when it is attached in the solid by an uptake). The sorption process basically reflects three kinds of chemical bonds; electrostatic attraction, covalent bond and van der Waals bond.



The sorption of radionuclides on different kinds of solid material from large volumes of waste aqueous solution is a potential process for reducing the transport of radionuclides to the environment. The adsorbents applied to decontaminate the effluents include clay minerals as bentonite clay (Lujaniene *et al.*, 2006; Xu *et al.*, 2008), activated carbon (Selvi *et al.*, 2001), carbon nanotubes (Li *et al.*, 2003), biosorbents such as microbial biomass (Tsezos and Volesky, 1981), metal oxides as titanium oxide ( $\text{TiO}_2$ ) (Zhang *et al.*, 2003) and zeolites (Chutia *et al.*, 2009). In addition, there are many other kinds of adsorbents used for water purification. For example, the removal of  $\text{Pb}^{2+}$ ,  $\text{Zn}^{2+}$  and  $\text{Cd}^{2+}$  using by-products steelmaking industry such as rolling mill scale and blast furnace sludge was studied by (Martin *et al.*, 2005). Moreover, the adsorption of  $\text{Ni}^{2+}$  and  $\text{Cu}^{2+}$  using oyster shell powder was studied experimentally by (Hsu, 2009).

A more recent alternative technique for treating the nuclear waste is to deposit the radioactive wastes in deep geological repositories in clay sediments (Gera *et al.*, 1993). However, Swedish Nuclear Fuel and Waste Management Company known as SKB (Svensk kärnbränslehantering AB), uses an effective multiple barrier method for final disposal of radioactive wastes from environment (Elam and Sundqvist, 2009; [www.skb.se](http://www.skb.se)). This method can be summarized as follows:

1. The radioactive wastes are encapsulated in canisters made of copper with iron insert (Figure 1.1a). The copper is used for corrosion resistance where as the iron strengthens the canister well.

2. These canisters are embedded in bentonite clay which is used as a buffer, that protects the canister against rock movement. Also it prevents water from leaking to the canister (Figure 1.1b).
3. The canisters are then emplaced in crystalline bedrock at a depth of 500 m (Figure 1.1c).
4. When the deposition is finished, the rock caverns and tunnels are sealed.

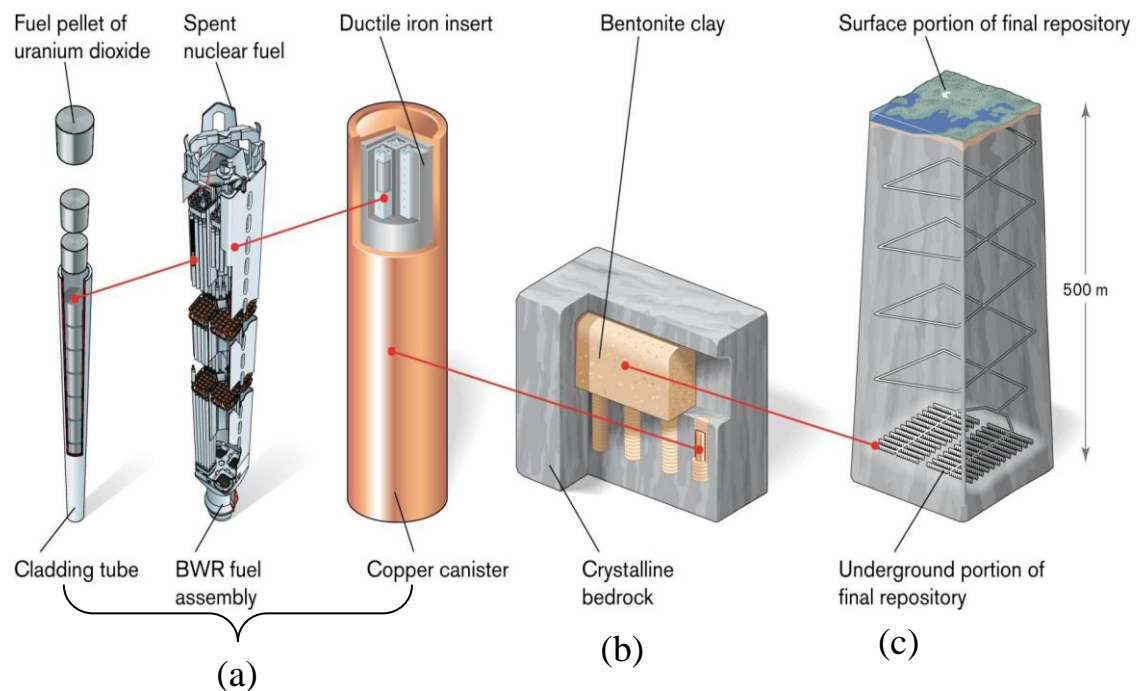


**Figure 1.1** SKB method for final disposal of radioactive wastes. (a) The copper canister with iron insert, (b) the bentonite clay as a buffer and backfill material and (c) the crystalline bedrock. ([www.quintessa.org](http://www.quintessa.org)).

The waste repository must guarantee the isolation of toxic and long lived radioactive wastes from environment. This efficient repository can be easily achieved by using bentonite which has the features that make it good host formations for radioactive wastes. Bentonite clay has good sorption

capability, so that if the canister is broken it could prevent the leakage of radioactive wastes from the canister. In addition, it has sufficient physical and chemical stability under high pressures, temperatures and other varying conditions of ground water. Therefore, bentonite can be used as backfill material between the engineered and natural barriers (Poernomo, 2010).

## **1.2 Literature Review**

Retention of ions on bentonite clay and their dependence on several parameters have been investigated both experimentally (Delattre-Louvel *et al.*, 1993; Lujaniene *et al.*, 2006; Sabodina *et al.*, 2006) and theoretically (Windt *et al.*, 2004; Bardbury and Baeyens, 2005). For example, the swelling properties of natural Mx-80 bentonite and Ca/Na montmorillonite have been studied experimentally and theoretically (Segad *et al.*, 2010).

In such a study, the theoretical data from dialysis and X-ray scattering experiments are confronted with the results from Monte Carlo calculations. A large swelling for monovalent counterions and a limited swelling for divalent counterions has been revealed. The limited swelling of clay, when the divalent counterions are in the aqueous solution, is explained upon the inclusion of the effect of ion-ion correlation.

Recently, the effect of valency on sorption process on Ca/Na montmorillonite using Monte Carlo simulations have been performed by (Qamhieh and Jönsson., The retention of multivalent pollutants in mineral layers, in preparation, 2015). It was found that for different valencies of counterions ( $M^{3+}$  and  $M^{4+}$ ) in the bulk solution of ground water, a competition for the charged surfaces exists. This competition depends on

the valency of counterion M, and as a result, the following results were noticed:

1.  $M^{n+}$  retention coefficient increases by increasing the surface charge density.
2.  $M^{n+}$  retention coefficient increases by decreasing the ratio  $Na^{1+}/Ca^{2+}$ .
3.  $M^{n+}$  retention decreases by increasing the bulk concentration of  $M^{n+}$ .

Moreover, Monte Carlo simulations have been performed to study the sorption of trivalent and tetravalent cations from sea water on bentonite clay (Maraaba, 2014). It was concluded that the retention coefficient increased by decreasing the multivalent concentration species in the bulk, temperature and ionic strength, whereas the surface charge density enhance the sorption process.

Various models and experimental studies were carried out to examine the sorption behavior of pentavalent cations on bentonite clay and their reliance on different factors as pentavalent concentration in the bulk solution, surface charge density of the clay platelet (pH), type of water, pressure, temperature and others. For example, the effects of changing pH on sorption process of Np(V) to montmorillonite was studied experimentally and by simulations by (Turner *et al.*, 1998). In that study, the Np(V) batch sorption experiment was carried out at a fixed mass to volume ratio (4 g/L), ionic strength (0.1 molal NaNO<sub>3</sub>) and initial Np(V) concentration of  $1 \times 10^{-6}$  molarity. The 2-site Diffuse-Layer Model (DLM) was used to predict the theoretical sorption values. However, a good agreement was found between the theoretical values from DLM model and

the experimental results. Accordingly, it was concluded that the sorption process is strongly affected by pH.

In addition, there are several studies investigating the influence of pH on the sorption process (Turner *et al.*, 1998; Zavarin *et al.*, 2012; Beall and Allard, 1981; Allard *et al.*, 1984; Torstenfelt *et al.*, 1988; Triay *et al.*, 1993). In those studies, the general behavior of the distribution coefficient of Np(V) tends to be constant for  $\text{pH} < 7$ , since in this interval the sorption is confined on the cation exchange which is a pH independent mechanism. Whereas, for  $\text{pH} > 7$ , the distribution coefficient increases by increasing pH. When the experiments were done in atmospheric pressure, the sorption process showed an increase with increasing pH up to pH value of 8 beyond which sorption decreases until pH value of 9.5 (Turner *et al.*, 1998; Bertetti *et al.*, 1998; Bertitte *et al.*, 1995). This decreasing behavior could be explained by the complexation of Np(V) element with the carbonate existing in the solution.

The impact of the metal ions concentration in the bulk solution has been examined in the studies of (Begg *et al.*, 2013; Xi *et al.*, 2011; Zavarin *et al.*, 2013). The sorption process in those studies was found to decrease by increasing the concentration of Pu(V), Sb(V) and Np(V) in the bulk, respectively.

Furthermore, the salinity of the solution will inhibit the sorption on montmorillonite. The sorption of Np(V) decreased by increasing the ionic strength of the solution through increasing the concentration of each of  $\text{CaCl}_2$ ,  $\text{MgCl}_2$ ,  $\text{NaCl}$  and  $\text{KCl}$  (Zavarin *et al.*, 2013). Such experimental

results are in agreement with the results obtained by (Zavarin *et al.*, 2012; Sabodina *et al.*, 2006; Kozai *et al.*, 1994; Lu *et al.*, 2009).

The temperature can also enhance or reduce the retention of pentavalent species. It was found that the sorption of As(V) decreases by increasing the temperature (Zahra *et al.*, 2009), while the sorption of Np(V) (Ohe *et al.*, 1993) and Pu(V) (Lu *et al.*, 2009) was found to increase by increasing temperature.

The sorption rate is also influenced strongly by the chosen adsorbent substance. For example, the sorption rate of Pu(V) on clays containing Fe or Mn minerals such as magnetite [ $\text{Fe}_3\text{O}_4$ ] and groutite [ $\alpha\text{-MnOOH}$ ] differs from clays with little or no Fe or Mn such as gibbsite [ $\text{Al}(\text{OH})_3$ ] and quartz [ $\text{SiO}_2$ ] (Begg *et al.*, 2013). This difference is explained by the surface reduction of Pu(V) element to Pu(IV) in the presence of reductant element on the clay which leads to a slower and stronger sorption. Moreover, the sorption rate of Pu(V) is affected by pH and ionic strength of the solution in a way that is different from goethite [ $\alpha\text{-FeOOH}$ ], magnetite and hematite [ $\alpha\text{-Fe}_2\text{O}_3$ ] (Zavarin *et al.*, 2012).

### 1.3 Objectives

The aims of this work are:

1. Applying Monte Carlo simulations in order to study the sorption process and to quantify the retention of pentavalent ions on bentonite clay when the waste water reservoir includes different types of cations.

2. Determining the effects of the following parameters on sorption process using Monte Carlo simulations:
  - Pentavalent concentration in the bulk.
  - Surface charge density.
  - Temperature.
  - Ionic strength.
3. Comparing the obtained results of this study with the available related experimental and theoretical ones.

## **Chapter Two**

### **Theoretical Background**

#### **2.1 Clay Minerals**

Clay minerals are described by hydrous aluminum silicate composition with a finite crystalline layered structure and very small particle size (less than 2 micrometers) (Robinson, 1962). They belong to the group of phyllosilicates and their structure is built of two distinct basic units (Grim, 1968; Meunier, 2005).

The tetrahedral sheet is a group of tetrahedron units having a silicon atom in the center and four oxygen atoms at the corners (Figure 2.1a), (Grim, 1968). They are linked to each other to form a tetrahedral sheet (Figure 2.1b) by sharing their atoms. The unshared atoms (the apical oxygen) of each tetrahedron point in the same direction and combine with the neighboring octahedral sheet. On the other hand, the octahedron unit in an octahedral sheet is composed of aluminum or magnesium in the center and six oxygen atoms or hydroxyl groups at the corners (Figure 2.2a), (Grim, 1968). All the bases of octahedrons are connected to form an octahedral sheet (Figure 2.2b).



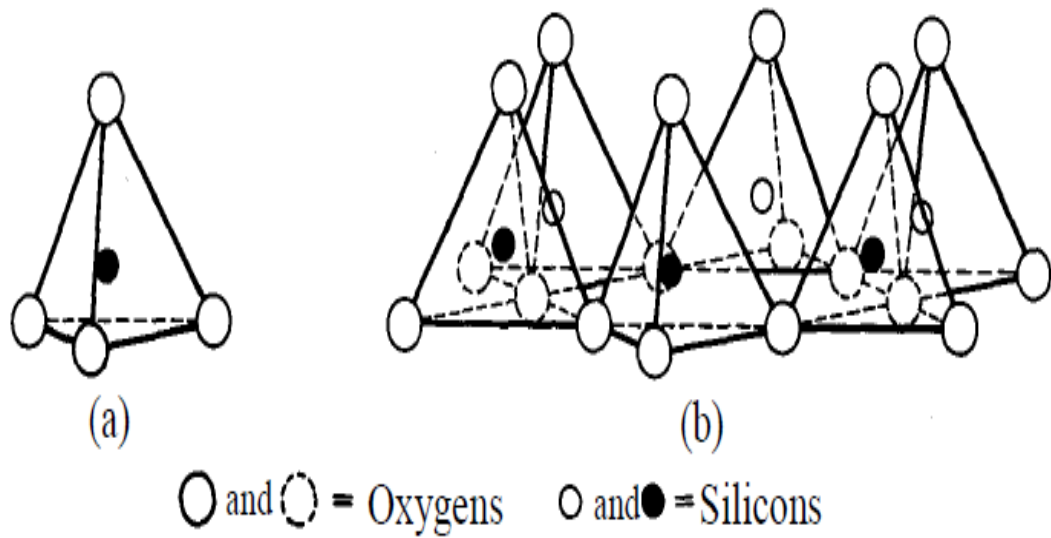


**Figure 2.1** Diagrammatic sketch illustrates (a) a single tetrahedron unit and (b) isometric view of tetrahedral sheet. (Grim, 1968).

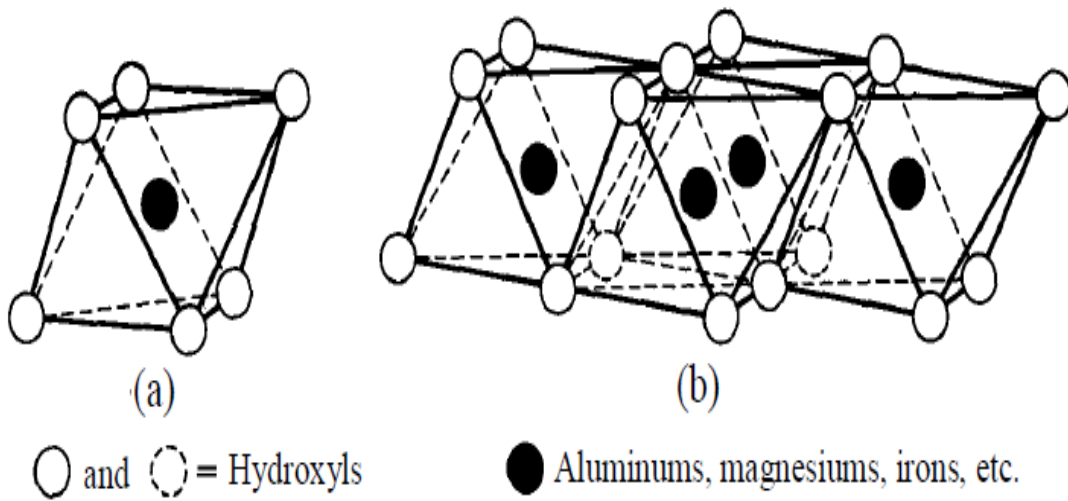


**Figure 2.2** Diagrammatic sketch illustrates (a) a single octahedron unit and (b) isometric view of octahedral sheet. (Grim, 1968).

Tetrahedral sheets (T) joined with octahedral sheets (O) in such a manner to form layered clays of two layer (1:1 = T:O), three layer (2:1 = T:O:T) and mixed layer which is a mixture of the two previous types. The clay minerals have been classified into different groups depending on many

factors (Meunier, 2005; Faure, 1998). Such factors include the number of clay layers, bonding joined layers together, various crystal structure resulted from the combinations of different sheets and cations, physical properties and the chemical compositions. The last one is found in octahedral sheet due to the ability of replacement of  $\text{Al}^{3+}$  atom by other cations, such as  $\text{Cr}^{3+}$ ,  $\text{Fe}^{3+}$  (trivalent) or  $\text{Mg}^{2+}$ ,  $\text{Fe}^{2+}$  (divalent). Accordingly, there are four distinct groups of clay minerals; smectite, vermiculite, kaolinite and illite. Particularly, clay minerals are widely used for adsorption of different kinds of pollutants from radioactive waste solutions (Eylem *et al.*, 1989). However, their contribution of controlling the concentrations of radioactive metals varies with solution pH, ionic strength, contact time, variation in mineralogy. The uptake of metal ions on clay minerals includes a variety of processes. These processes include ion exchange, inner- or outer-sphere surface complexation and surface precipitation.

## **2.2 Bentonite Clay Structure**

The main component of bentonite is montmorillonite which belongs to smectite group. It is 2:1 layer clay that consists of a central alumina octahedral sheet sandwiched by two silica tetrahedral sheets forming the unit cell formula  $\{\text{Al}_2(\text{OH})_2(\text{Si}_2\text{O}_5)_2\}$  (Van Olphen, 1977), Figure 2.3 (Grim, 1962). As can be seen, these three sheets form platelet of about 1 nm thick by sharing the oxygen atoms on the apices of silica tetrahedral sheet with hydroxyl or oxygen of the octahedral sheet (Robinson, 1962; Trauger, 1994), and together form a lamellar structure which illustrates an

electrical double layer model in the presence of aqueous electrolyte solution (Jeffery *et al.*, 1994).

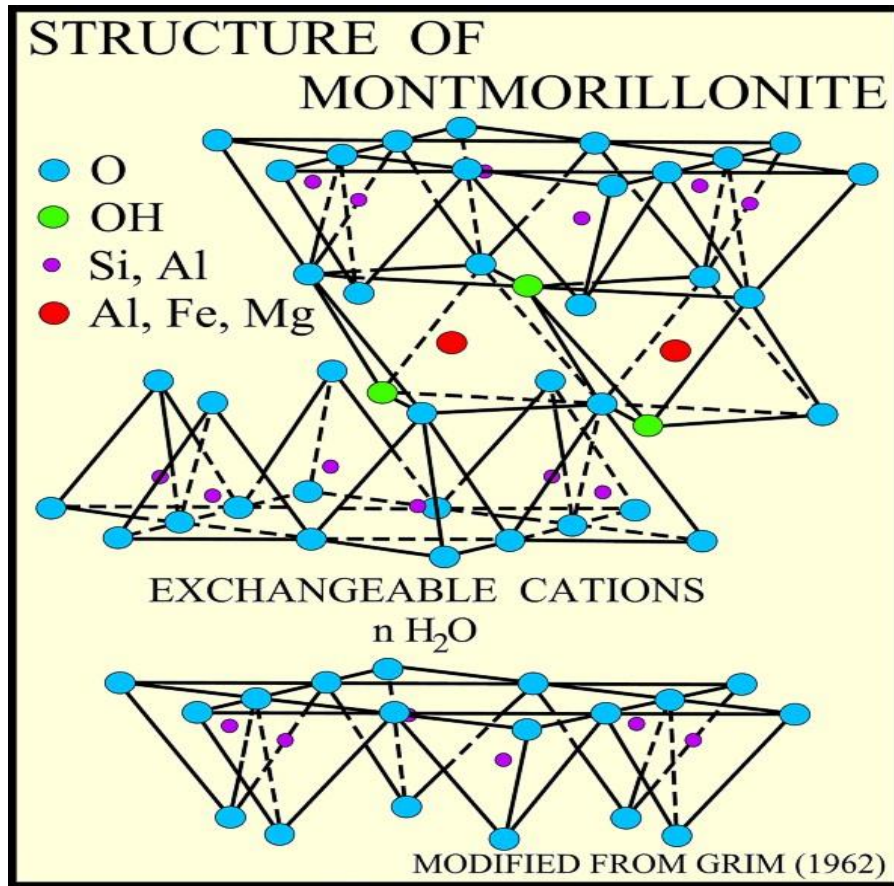


**Figure 2.3** Diagrammatic sketch of montmorillonite structure. (Grim, 1962).

Each bentonite platelet consists of two types of surfaces; external basal surfaces (faces) and edge surfaces (Jonsson *et al.*, 2008). These surfaces acquire a charge resulted from the substitution in the layers or from the reactions occurring at surface sites. The basal surfaces have a permanent negative charge attributed to isomorphous substitution in sheets, for example, the exchange of  $\text{Al}^{+3}$  with  $\text{Mg}^{+2}$  or  $\text{Fe}^{+2}$  in alumina octahedral or  $\text{Si}^{+4}$  with  $\text{Al}^{+3}$  in silica tetrahedral. On the other hand, the charge of the

edge surfaces which include broken bonds is determined by the reactions at the surfaces sites (Grim, 1953).

In the existence of water, the exposed alumina or silica coordinates with the water molecules (Stumm, 1992) according to the following reaction:



Where, J represents the metal ion at the surface. The surface site (JOH) resulted by forming bond between ion J and OH group posses a neutral charge. In the case of acidic solution,  $pH < 7$ , the charge on the edge surfaces is positive because of the association of hydroxyl group with the proton, as described in this reaction:



While in the basic solution,  $pH > 7$ , the edge surfaces have a negative charge due to the dissociation of the hydroxyl group as:



Therefore, the net negative value of the charge on the platelet surface will increase by increasing the solution pH.

The net negative charge on the platelet is neutralized by cations between layers, such as  $Ca^{+2}$ ,  $Na^{+1}$  and  $Mg^{+2}$  (Trauger, 1994; Grim, 1953). The clay platelets can arrange in three ways, namely, face to face (stacked platelets), edge to face and edge to edge (Meunier, 2005).

An identifying property of montmorillonite obtained from the weak interaction between the linked platelets is the expansion of crystal lattice when the polar molecules as water penetrate between the stacked platelets (Grim, 1953). Moreover, the additional features of bentonite including high

retention capability for cations, low permeability, plasticity, high swelling and large surface area candidate bentonite to serve as an effective barrier for retarding the radionuclide migration (Bartl and Czurda, 1991; Gera *et al.*, 1993; Trauger, 1994).

### **2.3 Diffuse Double Layer**

When a clay platelet is immersed into aqueous electrolyte solution, the cations will hold on the clay surface due to the electrostatic interaction, while the negatively charged particles tend to escape away from the charged surface in order to equal the solution concentration. The negative charge on the clay platelet and the cations distribution in the solution are commonly known as Diffuse Double Layer (DDL), (Mitchell, 1993).

The diffuse double layer (DDL) concept was developed from the principles of the electrical double layer that describes the differences of the electrical potential close to a charged surface. However, the DDL plays a significant role in the colloidal behavior and other surfaces inside electrolyte solution.

There are different models proposed to describe the structure of DDL. The earliest one is Helmholtz model (Figure 2.4), (Endo *et al.*, 2002; Mitchell, 1993; Van Olphen, 1977) in which two essential shortcomings were pointed out, namely:

- a. The interactions of anions and cations occurring away from the charged surface were neglected.
- b. The thickness and the extent of the diffuse double layer do not depend on the electrolyte concentration.

Therefore, the Helmholtz model is similar to the parallel plate capacitor; where its first plate forms from the clay surface of negative charge, and the second plate is the rigid cations linked opposite to the surface (Endo *et al.*, 2002). In this model, the electric potential falls pointedly from its extreme point on the charged surface to about worthless value on the center of the compact fixed layer that consists of adsorbed cations.

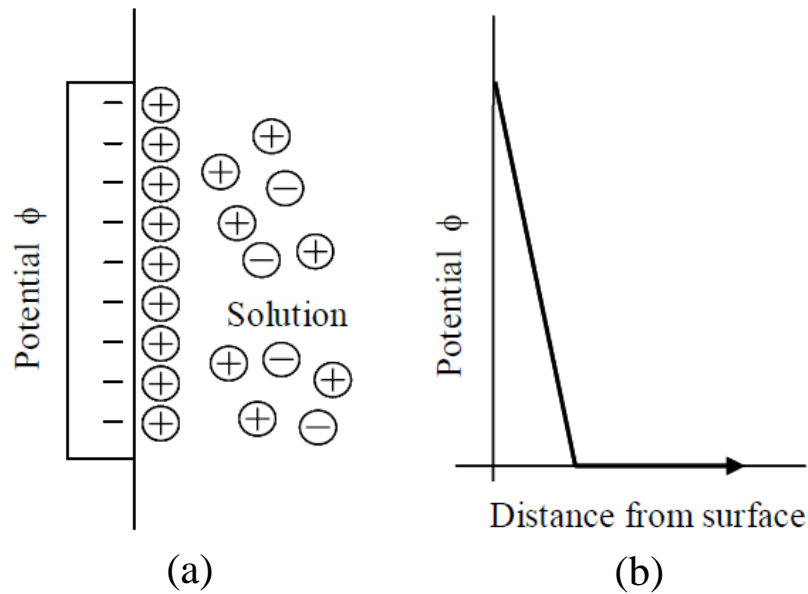


**Figure 2.4** (a) Helmholtz model which is identical to parallel plate capacitor.

(b) The electrical potential of the aqueous solution is falling sharply. (Mitchell, 1993).

Helmholtz model has been developed as a new model known Gouy and Champan model (Figure 2.5), (Mitchell, 1993). In this model, the electrical potential of the solution is decreasing exponentially from the charged surface and is extending to the aqueous solution due to the adsorbing of cations away from the surface. The calculated concentration of ions is very high at the charged surface because of the assumption of ionic charges

(Van Olphen, 1977; Mitchell, 1993). It should be pointed out that the ionic size in this model is not taken into consideration (Meunier, 2005).

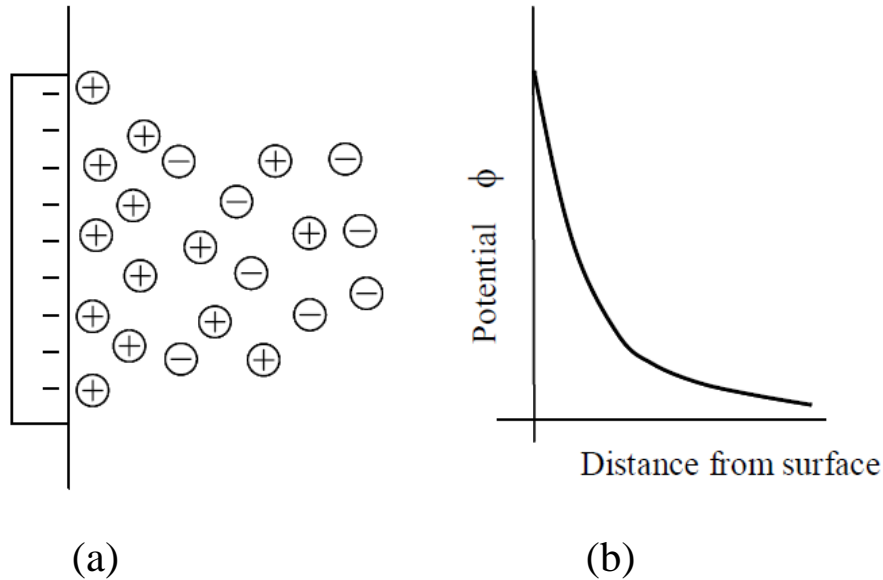


**Figure 2.5** (a) Gouy-Chapman model that has a diffuse layer.

(b) The electrical potential of the solution is decreasing exponentially from the charged surface to the extended solution. (Mitchell, 1993).

Moreover, the two previously mentioned models have been incorporated to another widely accepted model known as Stern Gouy-Chapman model (Figure 2.6), (Mitchell, 1993). This model is composed of two layers; the first one is a compact layer of cations of finite radius close to the negatively charged clay surface known Stern layer, identical to Helmholtz model. The other one is a diffuse layer of anions and cations extending into the electrolyte solution, identical to Gouy-Chapman model (Van Olphen, 1977; Mitchell, 1993). However, the thickness of the fixed Stern layer is the value of the radius of the attracted ion on the surface charge (Meunier, 2005).

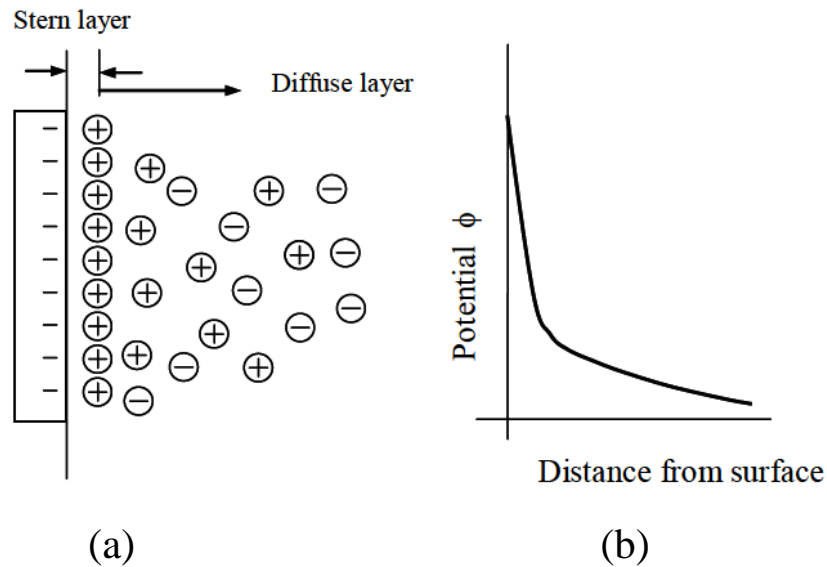


**Figure 2.6** (a) Stern Gouy-Champan model which forms of a compact layer of finite radius of cations known as Stern layer and a diffuse layer of anions and cations extending into the electrolyte solution. (b) The electrical potential decays with distance. (Mitchell, 1993).

## 2.4 Spatial Distribution of Counterions

Diffuse double layer can be represented mathematically by depending on the following assumptions (Mitchell, 1993):

1. Ions are considered to be point charges without interactions between opposite charges in the interlayer.
2. Charges on the clay surface due to isomorphous substitution are uniformly distributed.
3. The diffuse double layer is much smaller than the dimensions of the uniformly charged platelet surface.
4. The medium between surfaces has a constant permittivity value.



Poisson's equation gives the balance of charge in an electric field. For a dielectric homogenous medium, the general expression in one dimension is (Mitchell, 1993; Butt *et al.*, 2003):

$$\frac{d^2\phi}{dz^2} = \frac{-\rho_{ch}}{\epsilon_0\epsilon_r} \quad (2.4)$$

Where,  $\phi$  is the electrical potential opposite the charged surface,  $\rho_{ch}$  is the volume charge density,  $\epsilon_r$  is the relative permittivity constant of the medium and  $\epsilon_0$  is the dielectric constant in vacuum.

On the other hand, the distribution of ions in the electric field is represented by Boltzmann equation (Meunier, 2005; Mitchell, 1993; Butt *et al.*, 2003):

$$c_i = c_{i0} \exp\left(\frac{-v_i e \phi}{k_B T}\right) \quad (2.5)$$

Where,  $c_i$  is the ionic concentration of species  $i$ ,  $v_i$  is the ion valency,  $e$  is electron charge,  $c_{i0}$  is the ionic concentration at surface electrical potential ( $\phi_0$ ),  $k_B$  is Boltzmann constant and  $T$  is the absolute temperature.

The volume charge density may be expressed as:

$$\rho_{ch} = e \sum v_i c_i \quad (2.6)$$

Using equation (2.6), the Boltzmann equation becomes:

$$\rho_{ch} = e \sum v_i c_{i0} \exp\left(\frac{-v_i e \phi}{k_B T}\right) \quad (2.7)$$

Substituting equation (2.7) into equation (2.4) leads to the one-dimensional Poisson-Boltzmann formula (P-B):

$$\frac{d^2\phi}{dz^2} = \frac{-e \sum v_i c_{i0} \exp\left(\frac{-v_i e \phi}{k_B T}\right)}{\epsilon_0\epsilon_r} \quad (2.8)$$

For a solution with single cation and single anion species, 1:1 salt, such as NaCl and using clay surfaces of planer geometry, equation (2.8) can be solved as appeared in equations (2.9) and (2.10), (Mitchell, 1993; Butt *et al.*, 2003):

$$\phi = \phi_0 \exp(-Kz) \quad (2.9)$$

$$\exp(y/2) = \frac{\exp(y_0/2)+1+[\exp(y_0/2)-1] \exp(-Kz)}{\exp(y_0/2)+1-[\exp(y_0/2)-1] \exp(-Kz)} \quad (2.10)$$

Where,  $y = \frac{ve\phi}{k_B T}$  and  $y_0 = \frac{ve\phi_0}{k_B T}$ . The decay length (thickness of DDL) is denoted by  $1/K$  and is called the Debye-Huckel length, where:

$$K^2 = \frac{2c_0 e^2 v^2}{\epsilon_0 \epsilon_r k_B T}$$

Equations (2.9) and (2.10) represent the decay of electrical potential with increasing distance  $z$  from the charged surface at given surface electrical potential and electrolyte concentration (i.e.  $K$ ). However, equation (2.9) is valid at low potentials, especially when  $(ve\phi_0/k_B T) \ll 1$ , ( $y_0 \ll 1$ ), i.e. at room temperature, when  $\phi_0 < 25$  milli volt (mV). Otherwise, equation (2.10) is used at high potentials.

The distribution of cations, namely the electrical potential, in the Gouy-Champan model is generally decreasing exponentially by increasing distance from the charged surface (Figure 2.5b). Such distribution is applied to models that do not take the ion size into consideration. Moreover, when the volume of ion is included (Stern Gouy-Champan model), the concentration of cations is not perfectly exponential (Figure

2.6b). Instead, it is linear in the area near to the charged surface (Stern layer), while in the diffuse layer it becomes exponential (Meunier, 2005).

## **2.5 Sorption Process in Montmorillonite**

The sorption of ions on clay minerals is an important process to attenuate the migration of radionuclides. In this section, the mechanisms of sorption process onto montmorillonite, the distribution coefficient and the factors that affect the sorption capacity are discussed in the following subsections.

### **2.5.1 Sorption Mechanisms**

The sorption of ions on montmorillonite surface is controlled by two major mechanisms: the ion exchange and the surface complexation.

#### **a. Ion exchange**

The major cause of cation exchange on montmorillonite is the isomorphous substitution in the lattice structure, so that a negative charge will develop on planar surfaces which can be neutralized by the adsorbed cations. This mechanism is described in Figure 2.7 (Poernomo, 2010), in which the radionuclide is  $\text{Sr}^{2+}$ . When the cations are immersed into water they become hydrated, so the replacement capacity of the cations in the solution depends mainly on the valence and on the hydrated ionic size (Mitchell, 1993; McBride, 1994). The cations of higher valence replace the cations with lower one. However, if they have the same valence the cations of smaller hydrated size are preferred.

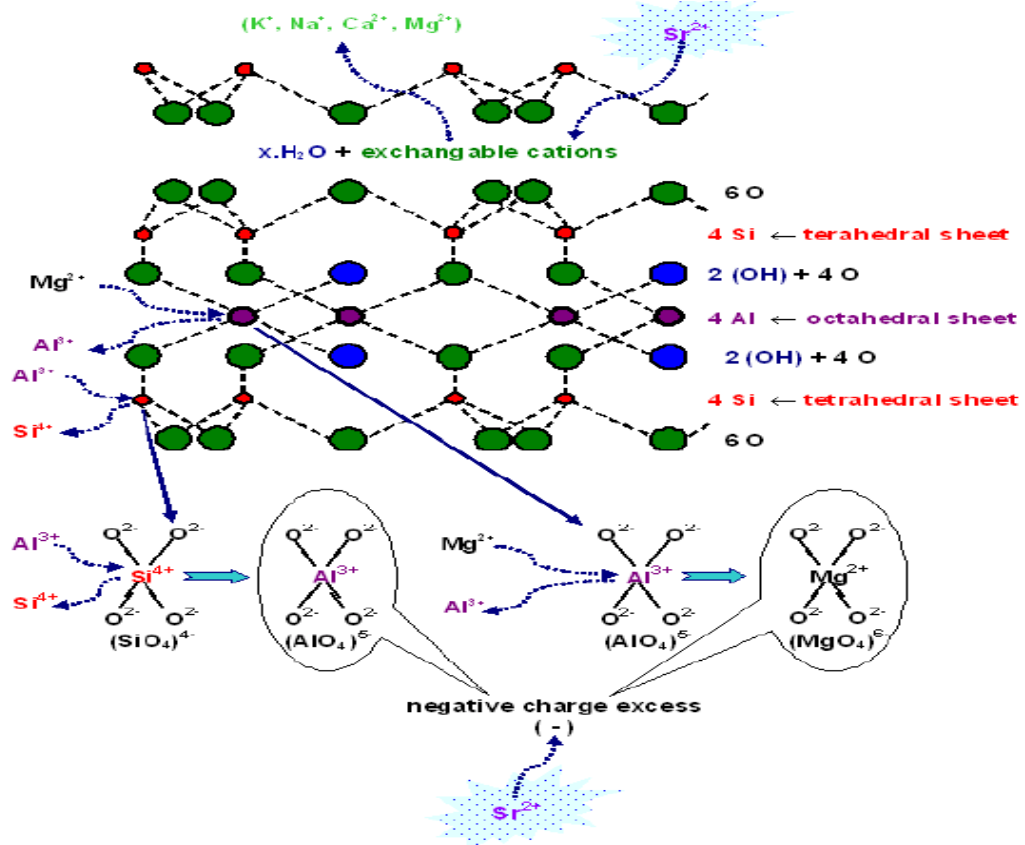


**Figure 2.7** Replaceability of exchangeable cations as Ca<sup>2+</sup>, Na<sup>+</sup> for Sr<sup>2+</sup> radionuclide and balancing the negative charge on the clay surface excess from isomorphous substitution of Al<sup>3+</sup> for Si<sup>4+</sup>, in tetrahedral, and Mg<sup>2+</sup> for Al<sup>3+</sup>, in octahedral, of bentonite minerals with Sr<sup>2+</sup>. (Poernomo, 2010).

Adsorption using cation exchange can be characterized by the following properties. It is pH-independent, taking place at the basal surfaces (in the interlayer) and occurring as a result of electrostatic interaction between the permanent charge and the ions in the solution. This mechanism can be described using either Donnan equilibrium or diffuse double layer (DDL) models, and it usually dominates at low pH (Dzombak and Hudson, 1995). The reaction of ion exchange (for example between L<sup>+</sup> and G<sup>+</sup>) can be expressed as (Fletcher and Sposito, 1989):

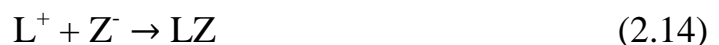


Where  $Z$  is the solid exchanger,  $L^+$  and  $G^+$  are ions in the solution.

### **b. Surface complexation**

Surface complexation includes formation of different bonds between the ions in the solution and the surface hydroxyl groups (OH) and O atoms leading to surface complexes (McBride *et al.*, 1991). It consists of two types of complexes, namely, inner-sphere and outer-sphere. If there are no water molecules between the ion and the functional group, the resulted reaction is an inner-sphere, and attributed to more covalent bonds. On the other hand, if at least there is one water molecule which is attached to the functional group, the complex is classified as an outer-sphere, and corresponds to electrostatic attraction (Cronstrand, 2005).

Surface complexation adsorption is pH-dependent, and is confined to the edge surfaces (Dzombak and Hudson, 1995). By returning to (Fletcher and Sposito, 1989), the hypothetical reactions of complexation method could be written as:



Where,  $Z$  is defined as a surface species.

### 2.5.2 Distribution Coefficient Concept

The sorption of radioactive metals on bentonite clay is determined by calculating the distribution coefficient  $k_d$  (ml/g) (Bartl and Czurda, 1991).

It is defined as:

$$k_d = \frac{\text{nuclide concentration in the solid phase}}{\text{nuclide concentration in the liquid phase}} \times \frac{V}{m} \quad (2.15)$$

Where, V is the volume of the solution in ml and m is the mass of the sorbent i.e. bentonite in gram.

Furthermore, the distribution coefficient can be expressed as (Khan *et al.*, 1995; Xu *et al.*, 2008; Li *et al.*, 2009):

$$k_d = \frac{c_i - c_e}{c_e} \times \frac{V}{m} \quad (2.16)$$

Where,  $c_i$  is the initial concentration and  $c_e$  is the equilibrium concentration of the adsorbed substance in the solution phase.

The retention coefficient ( $\gamma$ ) that represents the ion exchange or the ion competition is defined as (Qamhie and Jönsson., The retention of multivalent pollutants in mineral layers, in preparation, 2014):

$$\gamma = \frac{\langle c_{EDL}^{n+} \rangle + c_B^{n+}}{c_B^{n+}} \quad (2.17)$$

$\langle c_{EDL}^{n+} \rangle$  is the average electrical double layer (EDL) concentration of a cation that has valency (n) and  $c_B^{n+}$  is the cation concentration of valency (n) in the bulk solution.

Moreover, the retention coefficient ( $\gamma$ ) used to illustrate the sorption mechanism in (Maraaba, 2014) study is analogous to the coefficient applied in Qamhieh study, where:

$$\gamma = \frac{\langle c_{EDL}^{n+} \rangle}{c_B^{n+}} \quad (2.18)$$

The factor  $c_B^{n+}$  appeared in the numerator of equation (2.17) is neglected, since the multivalent species in the bulk solution are assumed to have low concentrations ( $10^{-8}$  to  $10^{-3}$  M). It is worth mention that, the  $\gamma$  is a dimensionless quantity, and proportions to the distribution coefficient  $k_d$ .

### 2.5.3 Factors Affecting Sorption Process

Sorption process in clays has been found to be affected by several factors, among:

- a. The substrate (bentonite, cement... etc) which attributed to the abundance of different minerals in the clay.
- b. The properties of the metals in the solution which include the valence or the hydrated radii (size).
- c. The solution conditions which containing the following parameters: pH, concentration of radioactive pollutants, ionic strength (salinity), temperature (T), pressure ( $P_{CO_2}$ ), contact time (t) and others (Khan *et al.*, 1995; Lujaniene *et al.*, 2006; Xu *et al.*, 2008).

## Chapter Three

### Model and Numerical Methodology

#### 3.1 Model System

Montmorillonite lamellar structure has been modeled as two infinite parallel planer surfaces with a net negative charge and separated by a tight water slit including balancing counterions and different added salts. In addition, the two surfaces have a uniform surface charge density ( $\sigma$ ) and separated by a distance  $h$  (Figure 3.1), (Segad *et al.*, 2010). This simpler planer model system is used by (Guldbrand *et al.*, 1984; Segad *et al.*, 2010; Maraaba, 2014).

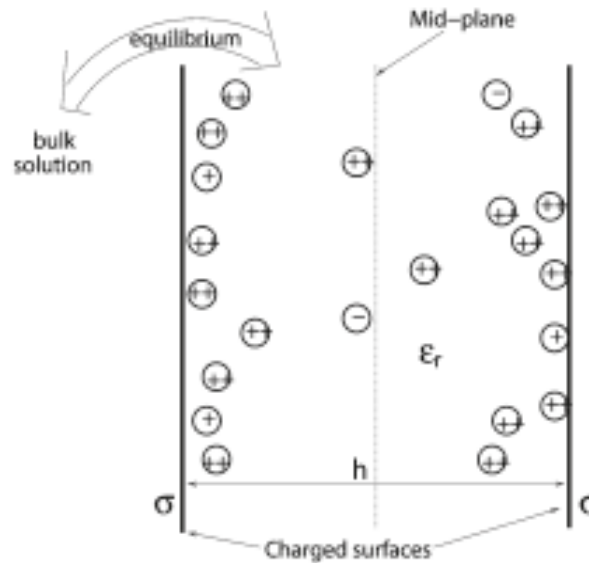


**Figure 3.1** Two infinite parallel walls of a uniform surface charge density a distance  $h$  apart. The ions are treated as charged hard spheres and water is modeled as a dielectric continuum with a relative dielectric permittivity constant  $\epsilon_r$ . (Segad *et al.*, 2010).

It is supposed that the lamellar structure is in contact and equilibrium with infinite brine reservoir of determined salt concentration (bulk solution). The primitive model used in this study has the following assumptions



(Torrie and Valleau, 1980; Valleau *et al.*, 1991; Jonsson *et al.*, 2008 and 2011):

1. The solvent (water) is treated as a dielectric continuum characterized by its relative dielectric permittivity constant ( $\epsilon_r = 78$  for water).
2. All charged species (cations) are described as charged hard spheres with a fixed diameter ( $d$ ) and are interacting with the walls.

Due to the resulted symmetry, the arrangement of ions is arbitrary. In addition, the dielectric constant is the same for the medium next to the surfaces and inside the solvent, that is the distribution of the surface charge over the walls is uniform (Torrie and Valleau, 1980). Accordingly, the effects of image charge are neglected producing surfaces with no dielectric discontinuity (Guldbrand *et al.*, 1984). Besides, periodic boundary conditions were set in directions parallel to the charged walls (Metropolis *et al.*, 1953) and the minimum image conventional technique was applied (Allen and Tildesley, 1987). Depending on the separation and the salt conditions, the number of ions ranged from 100 to 1000.

However, other simulations have been performed for a spherical geometry instead of planer geometry. They are modeled as cell model in which each particle is located in the centre of a spherical cell surrounded by the counterions (Marcus, 1954). For example, the cell model combined with the primitive model was performed by (Jonsson *et al.*, 2011) in order to determine the osmotic pressures for different colloidal dispersions. As a result, a surprising agreement between the results from the spherical and

the planar geometries was noticed. This reveals that the particle's geometry is of negligible influence in dispersions.

The interaction between two particles [ $U(r_{ij})$ ] is Coulombic. This ion-ion interaction can be written as (Segad *et al.*, 2010; Torrie and Valleau, 1980):

$$u(r) = \frac{v_i v_j e^2}{4 \pi \epsilon_0 \epsilon_r r} \quad \text{for } r > d \quad (3.1)$$

$$u(r) = \infty \quad \text{for } r \leq d \quad (3.2)$$

Where,  $v_i$  is the ion valency,  $r$  is the distance between the  $i$  and the  $j$  particles and  $d$  is the ion diameter (typical maximum diameter is 4Å). Furthermore, the ions interact with the charged surfaces, and an external potential is included to consider the interactions occurring outside the simulation box.

### 3.2 Method

The studies of the behavior and the properties of electrical double layer (EDL) systems are based on advanced techniques of statistical mechanics of liquid states. Some of these techniques are computer simulations such as Monte Carlo (MC) simulations (Torrie and Valleau, 1980 and 1982), integral equations (Jonsson *et al.*, 2008) and Poisson-Boltzman (P-B) equation (Derjaguin and Landau, 1941) which is one of the cornerstones of Derjaguin – Landau – Verwey – Overbeek (DLVO) theory. That theory deals with the electrostatic double layer interactions (McBride, 1997).

The latter technique is known as the mean field approximation for counterion distribution. Despite its accuracy, it fails when the dominant

counterions used in the system are divalent and at high surface charge density since it neglects the ion-ion correlations (Guldbrand *et al.*, 1984). The ion-ion correlations play an important role already with divalent ions and it is also emphasized with pentavalent ions in our study.

The first time of computer simulation of liquid was done by Metropolis (Metropolis *et al.*, 1953) at Los Alamos on the MANIAC computer, introducing Metropolis algorithm known as Monte Carlo method. That work has put the basis of recent “Monte Carlo simulation” in which a random input value is chosen for each task, depending on range of estimates. The model is calculated with reliance on this random number, the results are recorded and the operation is repeated thousands of times every time having different random value.

Monte Carlo is an efficient method for evaluating the properties of many body system and high dimension problems (Dongarra and Sullivan, 2000). The great advantage of this simulation that it can be implemented in several ensembles such as canonical ensemble (NVT), grand canonical ensemble ( $\mu$ VT), isobaric-isothermal ensemble (NPT) and others. Consequently and since Monte Carlo simulation is believed to be the most accurate method of the liquid state theories, this method was used in this study in order to solve the statistical mechanical system and to get dependable results. During the study, the simulations were performed in grand canonical (GC) ensemble when the lamellar structure is in equilibrium with the bulk solution.

### **3.2.1 Markov Chain**

The use of Metropolis algorithm needs to generate a sequence of connected random variables called Markov chain (Robert and Casella, 2010). A

Markov chain denoted by  $X^{(t)}$ :  $X^{(1)}$ ,  $X^{(2)}$  ...etc has a limiting distribution, and is constructed by a sequence of attempts that the outcome of each attempt achieves two conditions (Allen and Tildesley, 1987):

1. It must belong to the same limited set that containing the outcomes (state space set).
2. It is based just on the outcome of the attempt that preceding it directly.

### 3.2.2 Metropolis Algorithm

The standard Metropolis algorithm is used to carry out the simulations (Metropolis *et al.*, 1953) in grand canonical ensemble (Frenkel and Smit, 1996; Allen and Tildesley, 1987). It was introduced by Metropolis in 1953 and later was described by Beichl and Sullivan (Beichl and Sullivan, 2000). In the preceding section, the Metropolis algorithm was presented as a Markov process which is constructed randomly in such a manner that the probability of a particular point is proportional to Boltzmann factor [ $\exp(-\beta u(r))$ ], where  $\beta = 1/k_B T$ .

In order to build such a random process, the following approach has been proposed (Metropolis *et al.*, 1953):

1. Selecting a particle randomly and calculating its energy [ $u(r_h)$ ].
2. Changing the position of the particle by adding a random displacement to the old position and calculating the new energy [ $u(r_l)$ ].
3. Accepting the movement from state  $h$  to state  $l$  with probability:

$$p(h \rightarrow l) = \text{minimum}(1, \exp[-\beta(u(r_l) - u(r_h))]) \quad (3.3)$$

Where  $\Delta u_{lh} = u(r_l) - u(r_h)$ . The trial movement (displacement) is accepted or rejected according to the aforementioned acceptance probability as, if  $[u(r_l) < u(r_h), \Delta u_{lh} < 0]$  then  $p = 1$  and the movement is accepted. On the other hand, if  $[u(r_l) > u(r_h), \Delta u_{lh} > 0]$  then a random number  $\zeta$  is generated uniformly from the interval  $[0,1]$ . Now, the trial movement is accepted if  $\zeta < p_{(h \rightarrow l)}$ , otherwise, the trial is rejected. The probability that  $\zeta$  is less than the acceptance probability is  $\exp[-\beta \Delta u_{lh}]$ .

Based on Markov chain (Gelman *et al.*, 1996), if the move is accepted, the next iteration  $X^{(t+1)}$  has the value of  $r_l$  and the particle is moved to its new position. However, if it is unaccepted,  $X^{(t+1)}$  has the value of  $r_h$  (the old one) and the particle is returned to its old position.

To explain how the algorithm works when  $\Delta u_{lh}$  is greater than zero, look at Figure 3.2 (Allen and Tildesley, 1987). During the run, assume that a particular move is attempted and its  $\Delta U_{lh} > 0$ . Then, if a random number  $\zeta_1$  is selected, the move is acceptable with a probability of  $\exp[-\beta \Delta u_{lh}]$ . If  $\zeta_2$  is selected, the move is unacceptable (rejected). In this case, the system stays in state h and the particle is returned to its old position. However, the old configuration is considered as the new state in Markov chain.

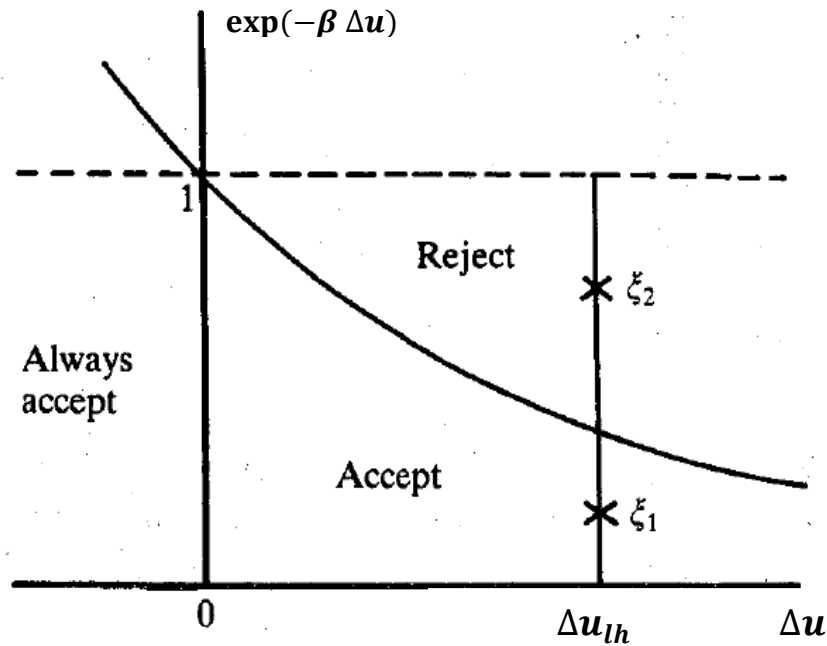


**Figure 3.2** The procedure of accepting or rejecting the trial moves in Monte Carlo simulation using Metropolis algorithm. That is, if  $\zeta_1$  is chosen, the attempt is accepted with probability of  $\exp[-\beta \Delta u_{th}]$ , while if  $\zeta_2$  is chosen, the attempt is rejected. (Allen and Tildesley, 1987).

### 3.2.3 Grand Canonical Ensemble

In this section, the statistical mechanical basis of grand canonical (GC) ensemble (section 3.2.3.1) and Monte Carlo (MC) implementation using grand canonical ensemble (section 3.2.3.2) are discussed.

#### 3.2.3.1 Statistical Mechanical Basis

Grand canonical ensemble is consisting of many systems each one has a fixed temperature and volume, its heat conducting walls are opened to particles transport. Therefore, the number of particles in a system can vary over all probable values (McQuarrie, 1976). In this kind of ensembles, the number of particles fluctuates. While, the volume (V), the temperature (T)

and the chemical potential ( $\mu$ ) are constants so it is called ( $\mu VT$ ) ensemble (Frenkel and Smit, 1996; Allen and Tildesley, 1987).

Grand canonical ensemble is a good choice in adsorption studies. The adsorbent particles are in equilibrium with the particles in the large reservoir at temperature  $T$ . To reach equilibrium condition, the chemical potential of the particles and the temperature outside and inside the adsorbent (clay) must be equal. Consequently, the thing that is exactly mimicked in GC ensemble is that the chemical potential and the temperature are imposed while the number of particles is let to fluctuate. Therefore, by knowing the  $T$  and  $\mu$  in the reservoir, the concentration of the particles inside the adsorbent at equilibrium can be determined (Frenkel and Smit, 1996).

The partition function ( $Z$ ) of grand canonical ensemble in a system containing interacting particles ( $N$ ) in a volume ( $V$ ) can be written as a summation, equation (3.4) or an integration forms (quasi-classical form), equation (3.5), (Frenkel and Smit, 1996; Allen and Tildesley, 1987; McQuarrie, 1976) as:

$$\begin{aligned} Z(\mu, V, T) &= \sum_N \sum_j \exp(N\mu\beta) \exp(-\beta u_{Nj}) \\ &= \sum_N \exp(N\mu\beta) Q(N, V, T) \end{aligned} \quad (3.4)$$

$$Z(\mu, V, T) = \sum_N \frac{\exp(N\mu\beta)}{\lambda^{3N} N!} \int_0^L \dots \int_0^L dr^N \exp[-\beta u(r^N)] \quad (3.5)$$

Where,  $Q(N, V, T)$  is the partition function of canonical ensemble,  $N$  is the number of particles,  $\lambda$  is the de Broglie wavelength and  $r$  is the radial distance.

It is appropriate to convert equation (3.5) to another form using scaled coordinates ( $S^N$ ) defined as:

$$r_i = L S_i \quad \text{for } i = 1, 2, 3, \dots, N \quad (3.6)$$

Where,  $L$  is the side of the simulation box. It is assumed that the system is included in a simulation box. If such box is a cubic, then  $L = V^{1/3}$  and equation (3.5) becomes (Frenkel and Smit, 1996):

$$Z(\mu, V, T) = \sum_{N=0}^{\infty} \frac{\exp(N\mu\beta) V^N}{\lambda^{3N} N!} \int ds^N \exp[-\beta u(S^N)] \quad (3.7)$$

In this study, the box used for simulation is a rectangular box. Its side is fixed and equals to 30 Angstrom. Accordingly,  $V^N$  in equation (3.7) can be replaced by  $(30)^{3N}$ .

Moreover,  $PV\beta$  is the appropriate function of thermodynamic (Allen and Tildesley, 1987; McQuarrie, 1976), since:

$$PV\beta = \ln Z(\mu, V, T) \quad (3.8)$$

Where,  $P$  is the pressure. In addition, the chemical potential can be derived from Helmholtz free energy ( $F$ ) (McQuarrie, 1976) as:

$$\mu = \left( \frac{\partial F}{\partial N} \right)_{T, V} \quad (3.9)$$

Where,  $F = U - TS$ ,  $U$  and  $S$  are the energy and entropy of the system, respectively. Besides, in grand canonical ensemble, the average of a physical quantity  $X$  such as energy ( $E$ ), pressure ( $P$ ) and number of ions ( $N$ ) can be calculated according to (Allen and Tildesley, 1987):



$$\langle X \rangle_{(\mu, V, T)} = \frac{\sum_{N=0}^{\infty} (N! \lambda^{3N})^{-1} \exp(N\mu\beta) V^N \int dS X(S) \exp[-\beta u(S)]}{Z(\mu, V, T)} \quad (3.10)$$

Since, during the MC simulation any property of the system is determined as its average in GC ensemble.

### 3.2.3.2 Monte Carlo Implementation

In GC ensemble, the lamellar system is in equilibrium with the bulk reservoir. So, the total chemical potential for each species of charged particles is the same in the double layer and in the bulk solution. Otherwise, the concentration of a given species in the double layer and in the bulk can differ.

The Markov chain in grand canonical Monte Carlo simulation (GCMC) is put in a way that the limiting distribution proportions to (Allen and Tildesley, 1987):

$$\propto \exp(-\beta [U(s) - \mu N]) - \ln N! - 3N \ln \lambda + N \ln V \quad (3.11)$$

In this ensemble, both the number of particles and energy fluctuate. The energy fluctuations are accomplished by displacement moves while the particle's number fluctuations are done by the addition or deletion of particles. In order to handle these fluctuations and to generate the Markov chain, the Norman and Filinov technique is used (Norman and Filinov, 1969). In this technique, there exist three distinct kinds of movements:

### a. Particle displacement

The displacement of particles is handled by the normal Metropolis algorithm as previously mentioned (section 3.2.2). The acceptance probability between the two states is:

$$p(h \rightarrow l) = \text{minimum} (1, \exp[-\beta \Delta u_{lh}]) \quad (3.12)$$

### b. Particle deletion (removal)

The acceptance probability of the removal of the randomly chosen particle is:

$$p(h \rightarrow l) = \text{minimum} (1, \frac{\lambda^{3N}}{V} \exp(-\beta[\mu + \Delta U_{lh}])) \quad (3.13)$$

### c. Particle creation (insertion)

The acceptance probability of addition particle randomly is:

$$p(h \rightarrow l) = \text{minimum}(1, \frac{V}{(N+1)\lambda^3} \exp(-\beta[\Delta U_{lh} - \mu])) \quad (3.14)$$

The acceptance or rejection of any of the aforementioned trials is determined by using the criterion described in (section 3.2.2). However, the displacement, destruction and insertion are selected randomly with the same probability (1/3), so that the chain converges fast.

## 3.2.4 Periodic Boundary Conditions

Calculations of MC were carried out for a collection of particles confined to a simulation box of a certain dimension. In order to reduce the surface effects, the simulation box is assumed to be periodic, composing of many boxes and each one is including N particles in a similar configuration (Metropolis *et al.*, 1953). When the particle moves in the main simulation

box, its image moves exactly in the same way in each of the periodic neighboring boxes (Allen and Tildesley, 1987). Therefore, as the particle leaves the original box, one of its periodic images will go through the counter face. A two dimensional system of such periodic conditions is shown in Figure 3.3 (Allen and Tildesley, 1987).

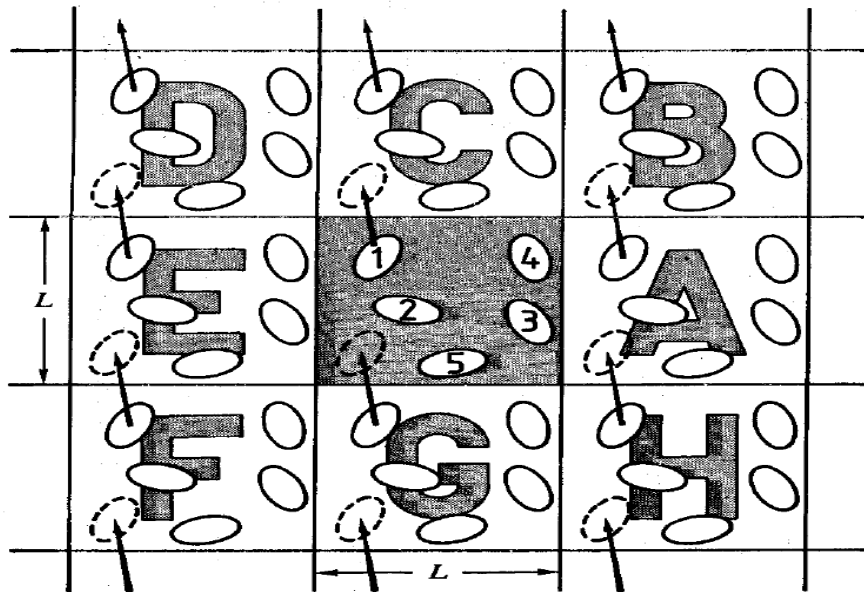


**Figure 3.3** A two-dimensional (2D) periodic model. The central square is the original one and the duplicate squares are labeled as A, B, C ... etc. When particle 1 moves through the edge of the square, its images 1A, 1B ... etc also move through their corresponding edges. In 3D periodic system, the particle is free to leave the box through six cubic faces. (Allen and Tildesley, 1987).

### 3.2.5 Minimum Image Conventional Technique

Depending on the periodic boundary conditions, the potential energy of the system can be calculated using minimum image conventional technique (Allen and Tildesley, 1987). The potential energy involving particle  $i$  can be calculated using that approximation as: particle  $i$  is considered to be set

at center of a region that has the same shape and size as the original simulation box. Then, particle  $i$  interacts with every particle whose center exists within the supposed region. For example, look at Figure 3.4 (Allen and Tildesley, 1987), particle 1 interacts with 2, 4E, 3E and 5C. In that approximation, the potential energy calculated by pairwise additive interactions contains  $\frac{1}{2} N (N-1)$  terms. The minimum image conventional approximation was used for the first time in simulation by (Metropolis et al., 1953) which resulted as a consequence of periodic boundary conditions.

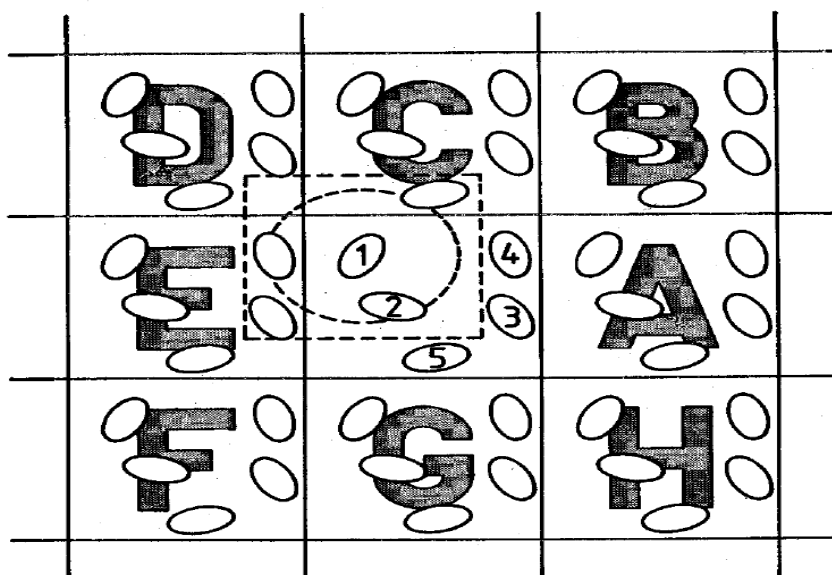


**Figure 3.4** Minimum image conventional technique in two-dimensional system. The potential energy containing particle 1 is the addition of the interaction pairs between particles of 1, 2, 4E, 3E and 5C. (Allen and Tildesley, 1987).

### 3.2.6 Methodology

The results present in this work were obtained by Monte Carlo simulations in grand canonical ensemble using Metropolis algorithm. In addition, the geometry of the bentonite platelets is planer and the primitive model is

used to describe the system. The lamellar structure is placed in an infinite reservoir of specified salt concentration at equilibrium condition.

The bulk solution includes varied concentrations of NaCl and CaCl<sub>2</sub> (normal species). They together represent a kind of water. For example, ground water is composed of 1mM NaCl + 4 mM CaCl<sub>2</sub>, while sea water is composed of 100 mM NaCl + 10 mM CaCl<sub>2</sub>. In addition, the bulk contains a little concentration of pentavalent cations (M<sup>5+</sup>) which are considered the radioactive substance. The abundance of mono-, di- and pentavalent species will form a competition to the charged surface of the clay platelet. Furthermore, these species will neutralize the charged surface in a different contribution.

The chemical potential ( $\mu$ ) used in this simulation consists of three parts as appeared in equation (3.15), (Hill, 1956):

$$\mu = k_B T \ln \lambda^3 + k_B T \ln c + \mu^{ex} \quad (3.15)$$

The first part is the standard ( $k_B T \ln \lambda^3$ ), the second part is the ideal ( $k_B T \ln c$ ) and the third part is the excess ( $\mu^{ex}$ ) chemical potentials. In this equation,  $\lambda = 1\text{\AA}$  and  $c$  is the average concentration of counterions (Molarity). It should be noted that, in GC ensemble, the overall chemical potential ( $\mu$ ) for both the bulk solution and the electrical double layer is the same.

The box used for performing the simulations is a rectangular with dimensions of (W×W×L), where W is the box size obtained through the running, while L is the separation distance between the two platelets which

is equal to 3 nm. However, all results are simulated for electrical double layer width of 3 nm but reasonable changes of the separation distance will not change the curves.

The mechanical properties of energy, pressure and number of counterions for each species are calculated during the MC simulations as the averages of grand canonical ensemble;  $\langle E \rangle$ ,  $\langle P \rangle$  and  $\langle N \rangle$ . In addition, the data of fraction, average electrical double layer concentration and the retention coefficient are shown as two dimensional curves.

**The fraction** ( $\alpha_{frac}$ ) of cation ( $M^{n+}$ ) in EDL is calculated using the following formula:

$$\alpha_{frac} = \frac{\langle N_{M^{n+}} \rangle \times n^+}{\langle N_{M^{1+}} \rangle \times (1^+) + \langle N_{M^{2+}} \rangle \times (2^+) + \dots + \langle N_{M^{n+}} \rangle \times n^+} \quad (3.16)$$

For example, the fraction of  $M^{5+}$  at specified surface charge density  $\sigma$ , bulk concentration  $c_B$  and constant temperature  $T$  in a bulk solution containing NaCl and  $CaCl_2$  is:

$$\alpha_{frac}(M^{5+}) = \frac{\langle N_{M^{5+}} \rangle \times 5^+}{\langle N_{Na^{1+}} \rangle \times (1^+) + \langle N_{Ca^{2+}} \rangle \times (2^+) + \langle N_{M^{5+}} \rangle \times 5^+} \quad (3.17)$$

In addition, **the average electrical double layer concentration**  $\langle c_{EDL} \rangle$ , in molarity unit (M), of cation  $M^{n+}$  was determined by employing the following formula:

$$\begin{aligned} \langle c_{EDL} \rangle &= \frac{\langle N_{M^{n+}} \rangle}{\text{box volume}} \times 1660.54 = \frac{\langle N_{M^{n+}} \rangle}{W \times W \times L} \times 1660.54 \\ &= \frac{\langle N_{M^{n+}} \rangle}{(W)^2 \times 30} \times 1660.54 \text{ (M)} \end{aligned} \quad (3.18)$$

Besides, the **retention coefficient** ( $\gamma$ ) can be defined as the competition or ion exchange coefficient. It can be written as the following definition:

$$\gamma = \frac{\langle c_{EDL}(M^{n+}) \rangle + c_B(M^{n+})}{c_B(M^{n+})} \quad (3.19)$$

Where,  $\gamma$  is a dimensionless coefficient and  $c_B$  is the concentration of  $M^{n+}$  cations in the bulk solution.

Moreover, the **counterion distribution** as function of distance  $z$  outside the charged surface has been plotted according to:

$$c(z) = \langle c_{EDL} \rangle g(r) \quad (3.20)$$

Where  $g(r)$  is the radial distribution function that determines the probability of find a particle separated by a distance  $r$  from other one. In GCMC simulations,  $g(r)$  is defined as the expectation value of delta function as the following formula (Hansen and McDonald, 2006):

$$g(r) = \left[ \frac{1}{\rho} \left\langle \frac{1}{N} \sum_{j=1}^N \sum_{i \neq j}^N \delta(r - r_j + r_i) \right\rangle \right] - 1 \quad (3.21)$$

Where  $\rho$  is the volume density of particles which is equal to  $N/V$ .

## Chapter Four

### Results and Discussion

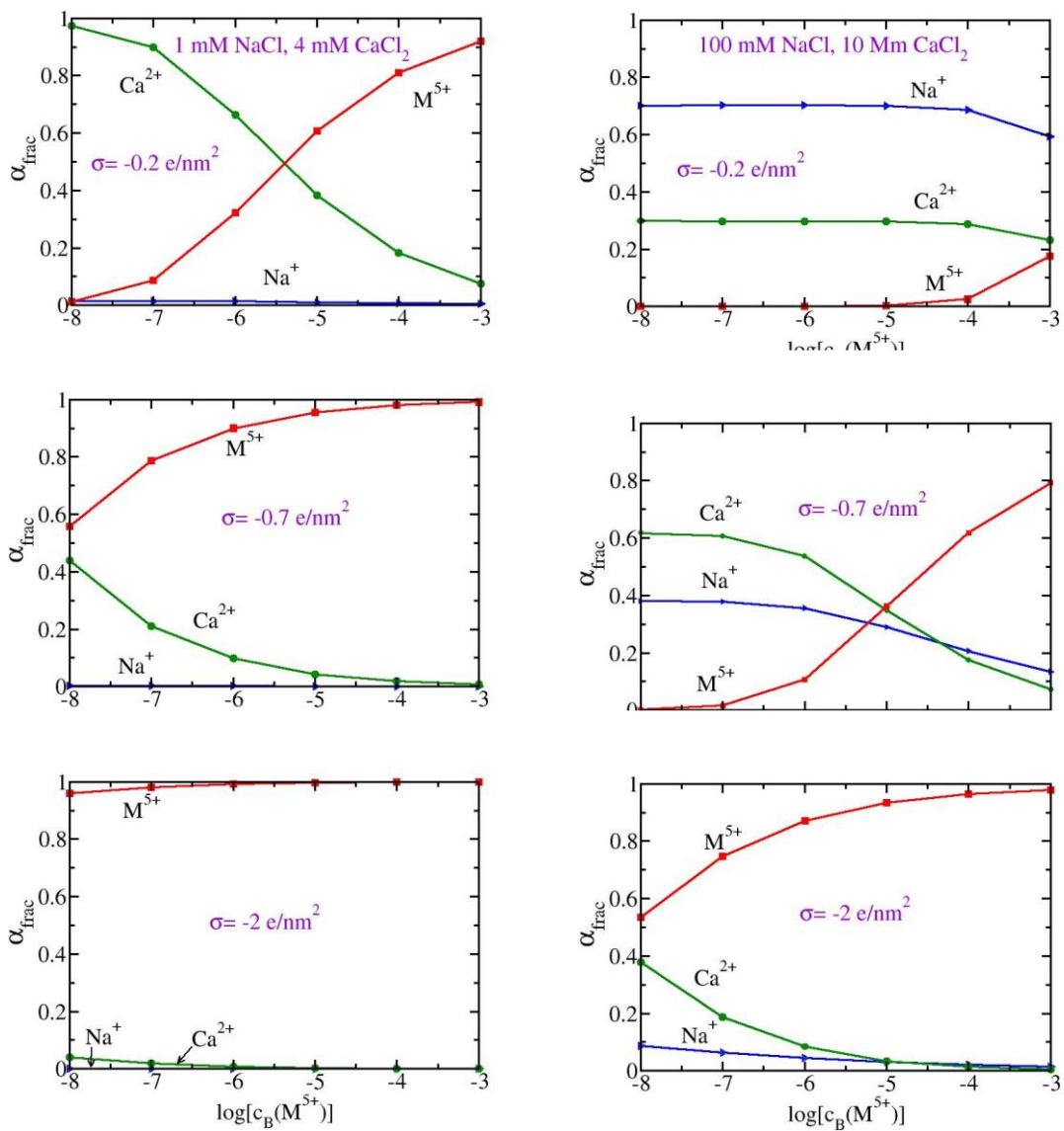
In this chapter, a series of Monte Carlo simulations has been used to investigate the sorption behavior of pentavalent ions to bentonite clay in two bulk systems. The first one includes 1mM NaCl, 4 mM CaCl<sub>2</sub>, representing ground water, while the other includes 100 mM NaCl, 10 mM CaCl<sub>2</sub>, representing sea water. In addition, the bulk contains an amount of pentavalent cations in various low concentrations ( $10^{-8}$  to  $10^{-3}$  M). All simulations have been performed in a separation distance of 3 nm between the two platelets. Moreover, during this study, it is assumed that the electrical double layer structure is in equilibrium with a bulk solution containing a known concentration of different neutralizing counterions. These counterions are referred to mono- (Na<sup>+</sup>), di- (Ca<sup>2+</sup>) and Pentavalent (M<sup>5+</sup>) cations in addition to monovalent anions (Cl<sup>-</sup>).

To shed some light on the factors that affect the assessment of sorption process, the following topics have been studied. The fraction of various counterions at different selected parameters (section 4.1), the impact of the pentavalent cations concentration in the bulk solution (section 4.2), the impact of the net negative surface charge density of the two separated platelets (section 4.3), the impact of increasing temperature (section 4.4) and the impact of changing the ionic strength of the electrolyte solution (section 4.5) in which the influence of changing the salinity of the solution has been studied throughout changing the CaCl<sub>2</sub> concentration (section 4.5.1) and changing the NaCl concentration (section 4.5.2).



#### 4.1 Fraction of Different Cations in EDL

The fraction of  $\text{Na}^+$ ,  $\text{Ca}^{2+}$  and  $\text{M}^{5+}$  cations in the EDL has been studied as a function of pentavalent cation concentration in the bulk solution. The pentavalent concentration was varied from  $10^{-8}$  to  $10^{-3}$  (M). The simulations were performed at room temperature (298 K) and at various values of surface charge densities ( $-0.2$ ,  $-0.7$ ,  $-2$ ,  $-3$ ,  $-4$  and  $-5$   $\text{e}/\text{nm}^2$ ).



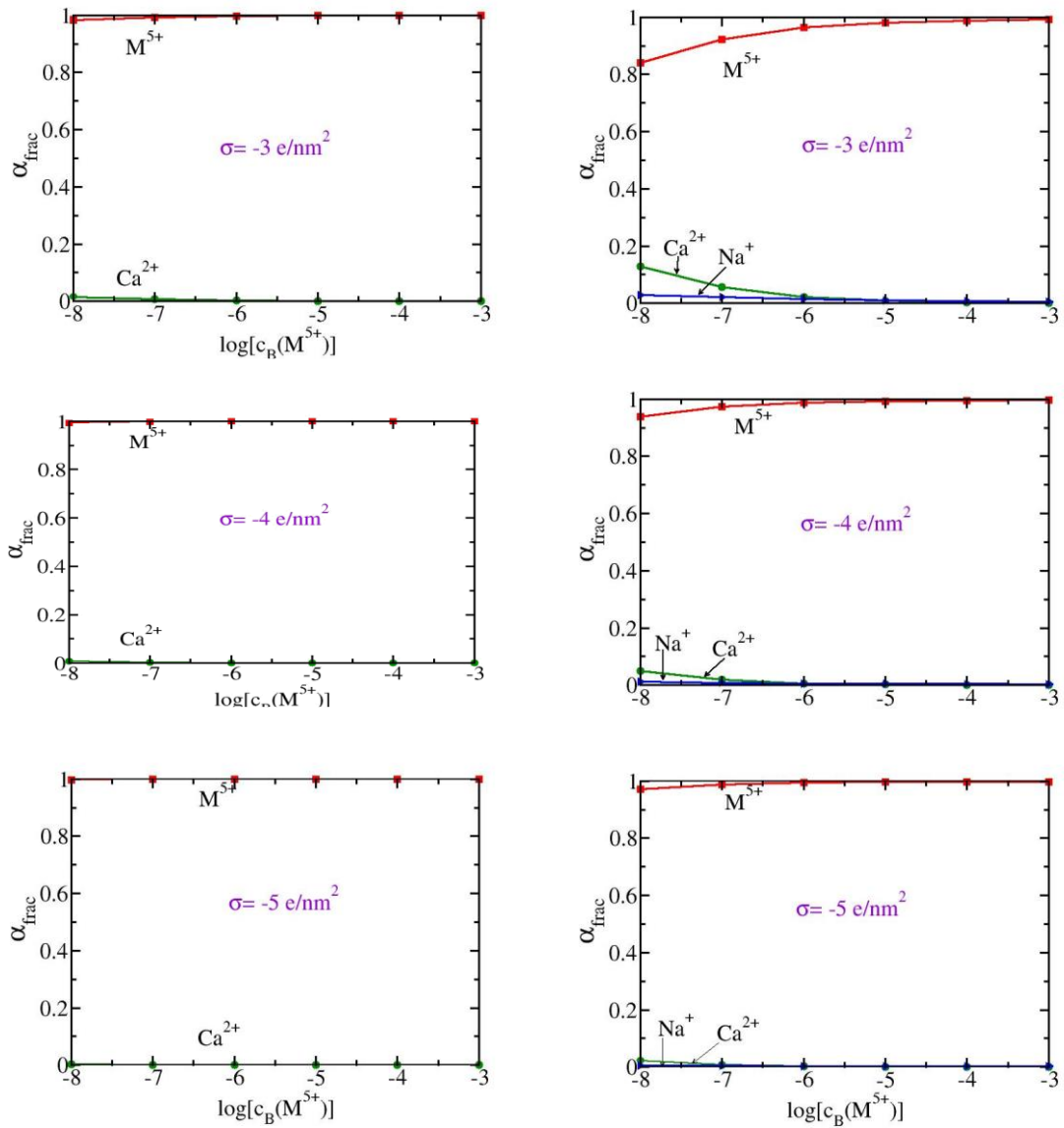


**Figure 4.1** Fraction of different counterions in the water slit as a function of pentavalent cations concentration in the bulk solutions. The slit is in equilibrium with a bulk including: a) 1 mM NaCl, 4 mM CaCl<sub>2</sub> (ground water), b) 100 mM NaCl, 10 mM CaCl<sub>2</sub> (sea water) and varied amount of pentavalent cations. The surface charge density has been varied as pointed in the graphs. The slit width is 3 nm.

It was shown that the fraction of pentavalent cation in the bulk solution of ground water increases by increasing its concentration in the bulk (Figure 4.1a). Concurrently, the fraction of Ca<sup>2+</sup> decreases drastically by increasing

the pentavalent concentration. Note that, the fraction of monovalent species in the electrical double layer is too low and difficult to be seen at higher surface charge densities. On the other hand, the bulk solution of sea water (Figure 4.1b) also illustrates that the fraction of  $\text{Na}^+$  and  $\text{Ca}^{2+}$  decreases by increasing the concentration of pentavalent cations in the bulk solution, while the fraction of  $\text{M}^{5+}$  increases. This behavior demonstrates the cation exchange sorption mechanism in which the pentavalent cations are adsorbed on the clay while  $\text{Ca}^{2+}$  and  $\text{Na}^+$  cations are released.

The fraction and the domination (the abundance) of the cations are influenced strongly by the magnitude of the surface charge density. In fact, the surface charge density ( $\sigma$ ) plays the key role in the competition between different cationic species for the charged surface. It is clearly obvious that by increasing the magnitude of surface charge density, the pentavalent species will be more abundant in the electrical double layer. For example, Figure 4.1a shows that at  $c_B = 10^{-7}$  M, the related values of fraction at  $\sigma = -0.2, -2$  and  $-5 \text{ e/nm}^2$  for pentavalent cations are  $\alpha_{\text{frac}} = 0.0868, 0.9807$  and  $0.9993$ , respectively. Also at  $c_B = 10^{-6}$  M, the related values of fraction at  $\sigma = -0.2, -2$  and  $-5 \text{ e/nm}^2$  are  $\alpha_{\text{frac}} = 0.0003, 0.8712$  and  $0.9949$ , respectively (Figure 4.1b).

According to the domination, Figure 4.1a represents that at surface charge density  $\sigma = -0.2 \text{ e/nm}^2$ ,  $10^{-5}$  M of pentavalent cations concentration in the bulk is enough for pentavalent cations to be dominant over monovalent and divalent ones in the electrical double layer. Above  $\sigma = -0.2 \text{ e/nm}^2$ , pentavalent cation is completely dominant over other species at all

considered concentrations. Note that above  $\sigma = -2 \text{ e/nm}^2$  the fraction of monovalent cation disappears since its concentration is too small to appear in the plots. In contrast to sea water (Figure 4.1b) the fraction of  $\text{Na}^+$  appears at all surface charge densities.

For  $\sigma = -0.2 \text{ e/nm}^2$ , the monovalent cation is the dominant species in the electrical double layer as performed in Figure 4.1b. By increasing surface charge density to  $-0.7 \text{ e/nm}^2$ , pentavalent cation is the dominant one at  $c_B$  equals to  $10^{-5} \text{ M}$ . However, at other surface charge densities ( $\sigma = -2, -3, -4$  and  $-5 \text{ e/nm}^2$ ),  $\text{M}^{5+}$  is completely dominant over other species.

By increasing the magnitude of surface charge density, the abundance of pentavalent cations will be more in the electrical double layer and their fraction approximately equals to one. It is good to remark that, the fraction of pentavalent cations in ground water (Figure 4.1a) closes to the unity faster than in sea water (Figure 4.1b). For example, the fraction in ground water approaches to unity at  $\sigma = -3 \text{ e/nm}^2$ , while in sea water at  $\sigma = -5 \text{ e/nm}^2$ . Accordingly, the charged surface is neutralized by pentavalent cations in ground water faster than in sea water. That is, the salinity of the bulk solution reduces the sorption behavior.

## **4.2 Effect of Pentavalent Cations Concentration in the Two Bulk Solutions**

The average electrical double layer concentration and the retention coefficient of pentavalent cations have been studied over changing the pentavalent concentration in the aqueous solution at various amounts of surface charge density and at room temperature (298 K). The pentavalent

concentration was varied from  $10^{-8}$  to  $10^{-3}$  (M) in the aqueous solutions of 1mM NaCl, 4 mM  $\text{CaCl}_2$  (ground water) and 100 mM NaCl, 10 mM  $\text{CaCl}_2$  (sea water).

It is obvious in Figure 4.2 that the average electrical double layer concentration of pentavalent cations increases slightly by increasing the pentavalent concentration in the bulk up to saturation point. In addition, it explains how pentavalent cations are completely dominant the neutralization of the charged surface. Besides, by increasing the surface charge density ( $\sigma$ ), the average EDL concentration of  $\text{M}^{5+}$  cations increases. That results are similar to (Begg *et al.*, 2013) in which the concentration of Pu(V) on montmorillonite increases by increasing the concentration of Pu(V) in the solution from  $10^{-17}$  to  $10^{-6}$  (M).

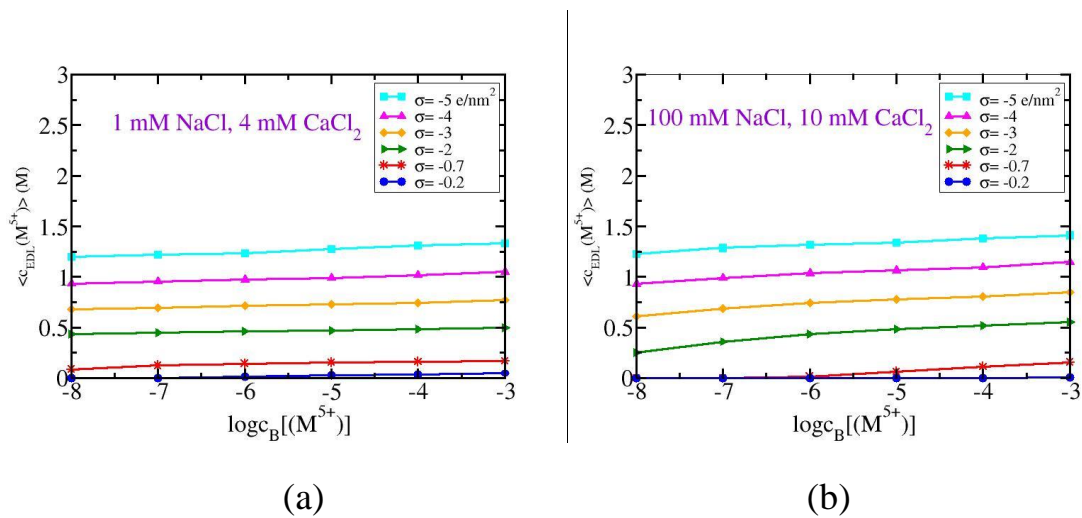


**Figure 4.2** Average electrical double layer concentration of the pentavalent cations as a function of their concentrations in the bulk. The bulk also includes a) 1 mM NaCl, 4 mM  $\text{CaCl}_2$  b) 100 mM NaCl, 10 mM  $\text{CaCl}_2$ . The surface charge density has been varied as pointed in the graphs. The slit width is 3 nm.

The spatial distribution of different counterions (counterion concentration) in the electrical double layer was plotted as a function of nanometric distance  $z$  from the charged surface (Figure 4.3). The bulk concentration of mono- and divalent species is 1 mM NaCl, 4 mM CaCl<sub>2</sub> (4.3a) and 100 mM NaCl, 10 mM CaCl<sub>2</sub> (4.3b), respectively with surface charge density of  $-3 \text{ e/nm}^2$ . The concentration of pentavalent cations is completely dominant over divalent ones, while the monovalent concentration is virtually zero (Figure 4.3a). Besides, in Figure 4.3b,  $M^{5+}$  distribution is the dominant.

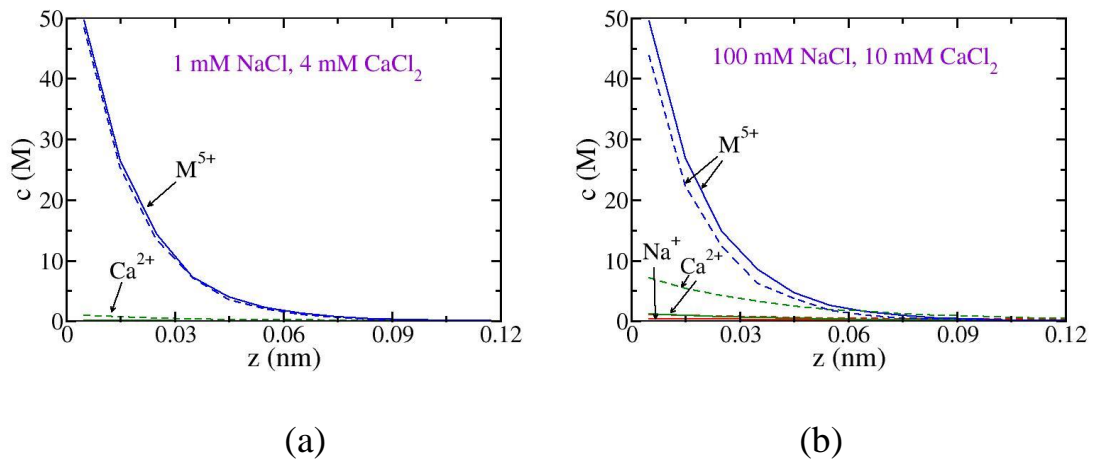


**Figure 4.3** Counterion distribution as a function of distance  $z$  outside the charged surface. Two different bulk systems are shown with a) 1 mM NaCl, 4 mM CaCl<sub>2</sub> b) 100 mM NaCl, 10 mM CaCl<sub>2</sub> and the concentration of pentavalent cations is increased from 0.00001 mM (dashed lines) to 0.001 mM (solid lines). The surface charge density is  $-3 \text{ e/nm}^2$  and the slit width is 3 nm.  $Na^+$  (red curves),  $Ca^{2+}$  (green curves) and  $M^{5+}$  (blue curves).

An increase of pentavalent concentration in the bulk solution from  $10^{-5}$  (dashed lines) to  $10^{-3}$  mM (solid lines) has a marginal increase of the

pentavalent distribution and a marginal decrease of the divalent distribution (Figure 4.3a). However, in Figure 4.3b this increase leads to a significant increase of pentavalent concentration in the double layer, a significant decrease of divalent cations and a marginal decrease of monovalent ones. In general, a rise of pentavalent concentration in the bulk solution produces an increase of  $M^{5+}$  distribution and a decrease of  $Na^+$  and  $Ca^{2+}$  distributions.

The distribution of pentavalent cations from the charged surface in ground water (Figure 4.4a) and in sea water (Figure 4.4b) decays exponentially. Such behavior was found for the cations distribution in the models that don't consider the ion size (Figure 2.5b), sections of (2.3 and 2.4). Figure 4.4 again explains how the electrical double layer will be saturated with pentavalent cations. It is clear that a shift from 0.00001 to 0.0001 and to 0.001 mM in the bulk affects the electrical double layer content of pentavalent cations obviously. However, additional increase is enough to make the double layer saturated by pentavalent cations. That is, any increase above 0.001 of the bulk concentration has a very minor influence on the EDL concentration.

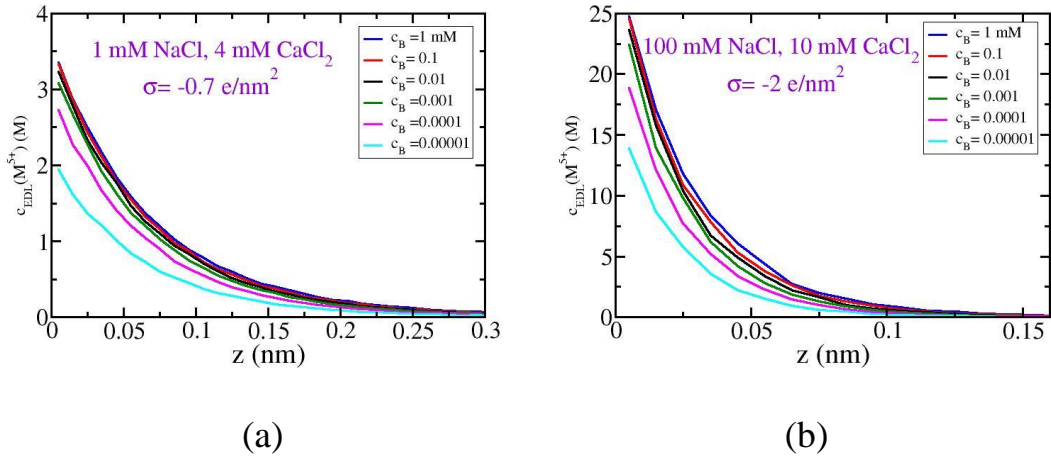


**Figure 4.4** Pentavalent cations distribution as a function of distance  $z$  outside the charged surface. Two different bulk systems are shown with a) 1 mM NaCl, 4 mM  $\text{CaCl}_2$  b) 100 mM NaCl, 10 mM  $\text{CaCl}_2$  and different values of pentavalent cations concentration as pointed in the graphs. The slit width is 3 nm and the surface charge density is a)  $-0.7 \text{ e/nm}^2$  b)  $-2 \text{ e/nm}^2$ .

The retention coefficient of pentavalent cations as a function of their concentration in the bulk solution is presented in Figure 4.5. The formula used to express the retention coefficient is:

$$\gamma = \frac{\langle c_{EDL}(M^{5+}) \rangle + c_B(M^{5+})}{c_B(M^{5+})}$$

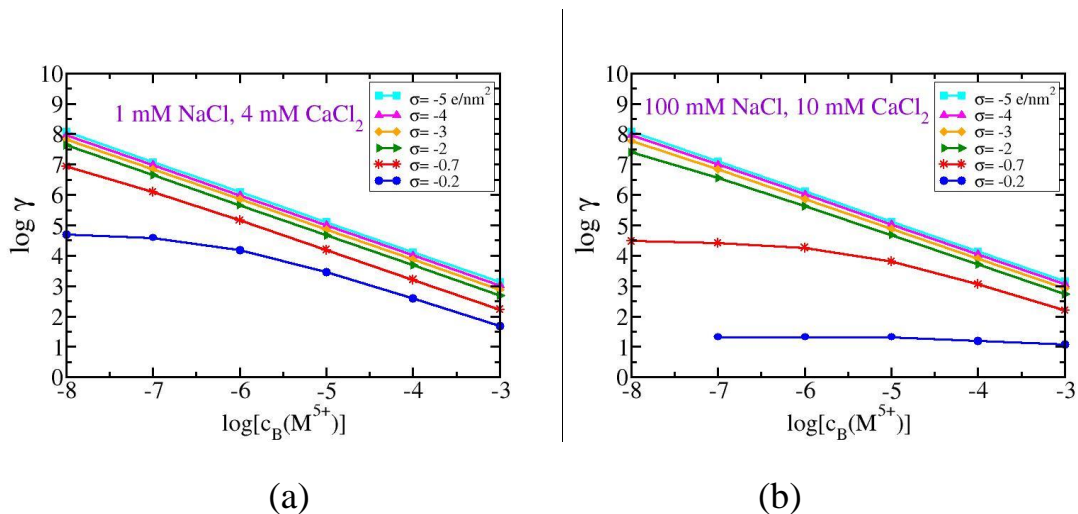


**Figure 4.5** The retention coefficient calculated from the curves in Figure 4.2.



The general trend of the retention coefficient becomes less as the pentavalent concentration increases. The nature of retention behavior is dependent on the surface charge density as clarified in Figure 4.5. The retention coefficient, at low surface charge densities, is approximately constant at low concentrations of pentavalent cations, and then reduces linearly. For example, Figure 4.5a shows that, at  $\sigma = -0.2 \text{ e/nm}^2$  the retention has a constant value of 4.6 between  $10^{-8}$  and  $10^{-7}$  M and then nearly at concentration of  $10^{-6}$  M, it decreases linearly. Whereas, Figure 4.5b displays that, at  $\sigma = -0.2 \text{ e/nm}^2$  the retention approximately has a constant value at all bulk concentrations. However, at  $\sigma = -0.7 \text{ e/nm}^2$ , the retention is almost constant between  $10^{-8}$  and  $10^{-6}$  M, and then decreases linearly.

In contrast, at high magnitudes of surface charge density, such as ( $\sigma = -3, -4$  and  $-5 \text{ e/nm}^2$ ) the retention coefficient reduces linearly with increasing the  $M^{5+}$  concentration from  $10^{-8}$  to  $10^{-3}$  (M). The linearity behavior of retention coefficient as a function of  $\log [c_B(M^{5+})]$  reveals that the surface is neutralized by the pentavalent cations only as shown in Figure 4.2. Moreover, at high values of surface charge density the retention coefficient becomes independent of the type of water.

Many batch sorption experiments were conducted to study the retention coefficient of different pentavalent radionuclides. In which, the sorption coefficient of Pu(V) on montmorillonite (Begg *et al.*, 2013), Sb(V) on bentonite (Xi *et al.*, 2011) and Np(V) on Na-montmorillonite (Zavarin *et*

*al.*, 2013) is decreasing by increasing their concentration in the aqueous solution.

### 4.3 Effect of Surface Charge Density

The dependence of sorption process of pentavalent cations on surface charge density ( $\sigma$ ) of the two platelets on bentonite has been studied by varying the values of surface charge density. They were changed from -0.2 to -13  $e/nm^2$  in a bulk solution of 1 mM NaCl, 4 mM  $CaCl_2$  (ground water) and from -0.7 to -13  $e/nm^2$  in a bulk solution of 100 mM NaCl, 10 mM  $CaCl_2$  (sea water). The bulk also includes a determined concentration of pentavalent cations ranging from  $10^{-8}$  to  $10^{-3}$  (M). The simulations were performed at fixed temperature of 298 K (room temperature).

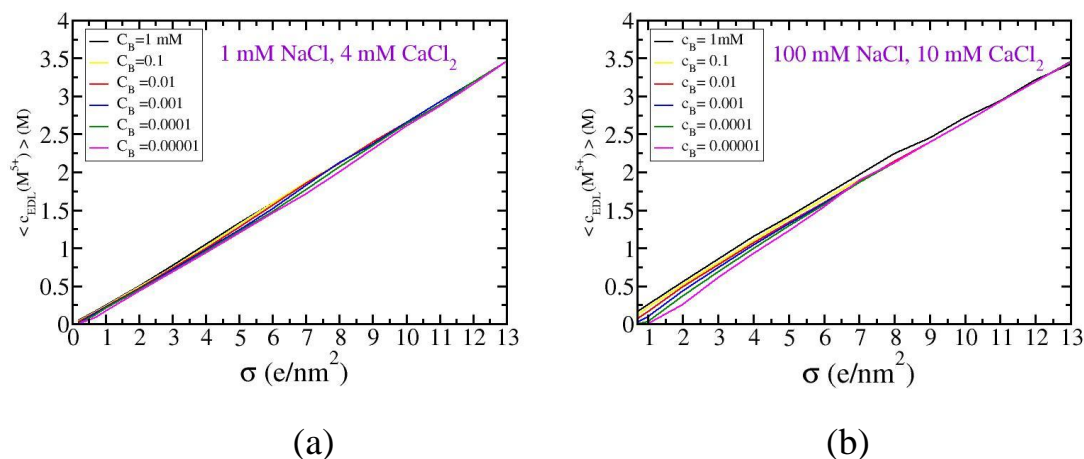


**Figure 4.6** Average electrical double layer concentration of pentavalent cations as a function of surface charge density of the two separated walls. The bulk concentration of pentavalent cations has been varied as pointed in the graphs. The bulk also includes a) 1 mM NaCl, 4 mM  $CaCl_2$  b) 100 mM NaCl, 10 mM  $CaCl_2$ .

Figure 4.6 shows that, the average electrical double layer concentration of pentavalent cations in the two different bulk systems has almost a linear behavior for all pentavalent cations concentrations and at all measured values of surface charge density. Besides, it increases with the magnitudes of surface charge density up to  $-13 \text{ e/nm}^2$ . In addition, the curves shown in Figure 4.6a are very close to each other, and seem to be one line. This means that, the average EDL concentration is independent of the bulk concentration at all surface charge densities. On the other hand, the average concentration shown in Figure 4.6b is slightly dependent on bulk concentration at low surface charge densities, while at high values it doesn't depend on the bulk concentrations.

The average EDL concentration of a) trivalent and b) tetravalent cations in a bulk concentration of 100 mM NaCl, 10 mM CaCl<sub>2</sub> is illustrated in Figure 4.7 taken from (Maraaba, 2014). By comparing the results of this study (Figure 4.6b) with the previous study (Figure 4.7), one can conclude that the average concentrations of  $M^{5+}$  curves are more closer to each other than  $M^{3+}$  and  $M^{4+}$  also  $M^{4+}$  curves are more closer than  $M^{3+}$ . This behavior reveals that, by increasing the valency of radionuclide, the average EDL concentration as a function of surface charge density will be independent of the bulk concentration.

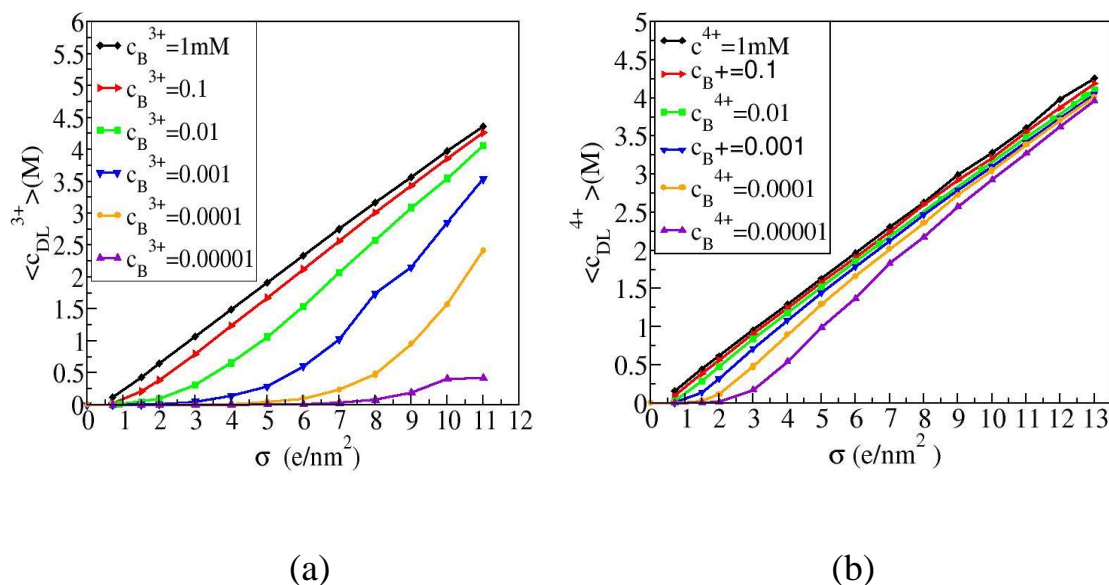


**Figure 4.7** Average electrical double layer concentration of a) trivalent ( $M^{3+}$ ) b) tetravalent ( $M^{4+}$ ) cations as a function of surface charge density. The bulk contains 100 mM NaCl, 10 mM  $CaCl_2$  and varied amount of the multivalent species.

The counterion concentration in the electrical double layer was plotted as a function of distance  $z$  outside the charged surface in Figure 4.8. The bulk solution includes 100 mM NaCl, 10 mM  $CaCl_2$  in addition to 0.0001 mM of pentavalent cations. The result indicates that by increasing the magnitudes of  $\sigma$  from -2 to -3 and to -4  $e/nm^2$ , the electrical double layer content of  $M^{5+}$  increases clearly. On the other hand, the concentration of mono- and divalent cations decreases. Moreover, the concentration of pentavalent ions in EDL is decreasing exponentially.

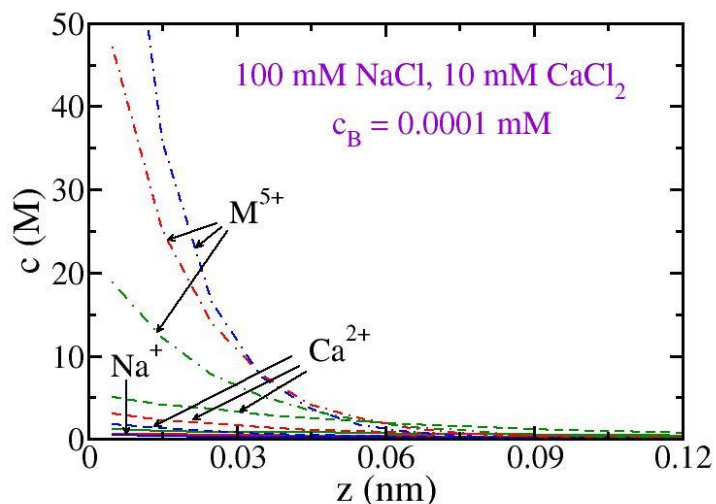


**Figure 4.8** Counterion distribution as a function of distance  $z$  outside the charged surface. The bulk solution contains 100 mM NaCl, 10 mM CaCl<sub>2</sub> and 0.0001 mM of pentavalent cations. The surface charge density has been varied; green curves =  $-2$  e/nm<sup>2</sup>, red curves =  $-3$  e/nm<sup>2</sup> and blue curves =  $-4$  e/nm<sup>2</sup>. The slit width is 3 nm. Na<sup>+</sup> (solid lines), Ca<sup>2+</sup> (dashed lines) and M<sup>5+</sup> (dot-dashed lines).

The sorption data of pentavalent cations calculated by changing the magnitude of surface charge density has been presented in Figure 4.9. Obviously, by increasing the  $|\sigma|$  in ground water (Figure 4.9a) and in sea water (Figure 4.9b), the retention coefficient increases and reaches a saturation value quickly. However, a low surface charge density is required for saturation in both cases;  $1$  e/nm<sup>2</sup> for ground water and  $2$  e/nm<sup>2</sup> for sea water. Besides, the saturation value (at all bulk concentrations) is independent of the type of water. In addition, by increasing the bulk concentration the retention decreases.

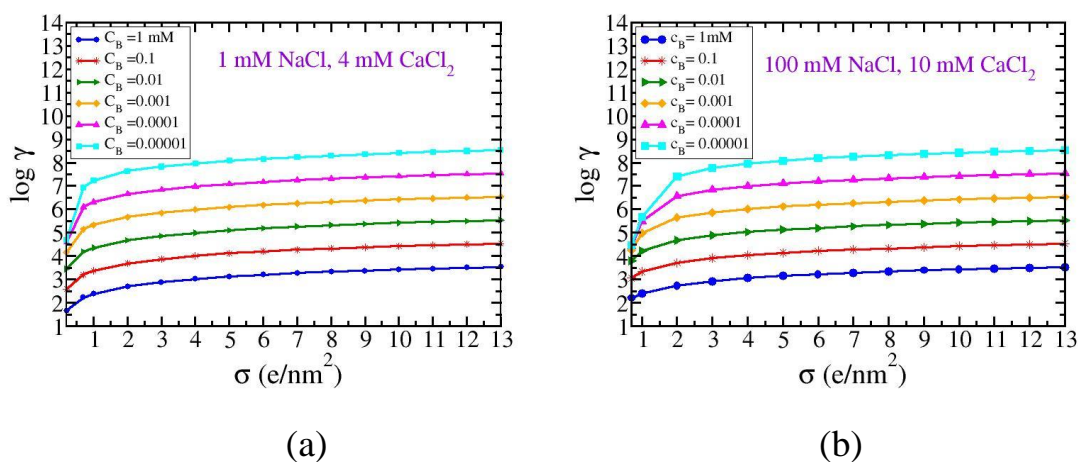


**Figure 4.9** The retention coefficient calculated from the curves in Figure 4.6.

Certainly, there is a direct relation between the surface charge density of the platelets and the solution pH. By increasing the solution pH, the net negative surface charge density will increase (section 2.2). The sorption data of pentavalent cations on bentonite clay presented in Figure 4.9 strongly agree with various experimental studies.

Our results of sorption behavior are consistent with (Zavarin *et al.*, 2012) when the studied pH range is 5 to 8. But, an incompatibility was found when the pH range is 3 to 5, a constant sorption behavior of Np(V) is observed. That study attributed the constant sorption to the predomination of ion exchange when the pH range is 3 to 5 which has no pH dependence. While when pH is greater than 5, the surface complexation is the dominant. Besides, a good agreement was found with studies of (Turner *et al.*, 1998; Bertetti *et al.*, 1998; Bertetti *et al.*, 1995). That studies have a continuous increasing of Np(V) sorption correlated with an increase in pH of the solution from 5 to 11 in the first two studies and from 6.5 to 10 in the last one. The sorption of Np(V) in the previous studies is controlling by surface

complexation mechanism. The ion exchange is suppressed by using 0.1 molal of  $\text{NaNO}_3$  in the solution (high ionic strength). Therefore, the sorption behavior when pH is less than 5 doesn't appear.

In summary, the results showed in our study go with different experiments which have been conducted to study the pH dependence of Np(V) sorption on montmorillonite. These studies are summarized in Figure 4.10.

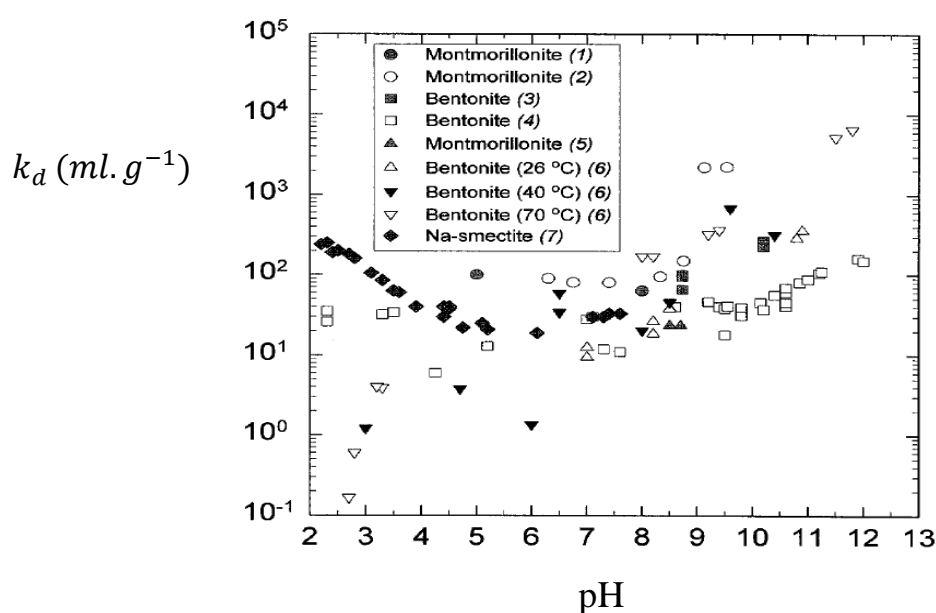


**Figure 4.10** Comparison of sorption data for Np(V) actinide on bentonite and montmorillonite from different studies. Data sources contain: (1) (Beall and Allard, 1981), (2) (Allard *et al.*, 1984), (3) (Torstenfelt *et al.*, 1988), (4) (Sakamoto *et al.*, 1990), (5) (Triay *et al.*, 1993), (6) (Ohe *et al.*, 1993) and (7) (Kozai, 1994). (Turner *et al.*, 1998).

Figure 4.10 shows that, the observed behavior of distribution coefficient of Np(V) generally tends to be relatively constant at pH less than 7 and then increases by a further increase in pH (Beall and Allard, 1981; Allard *et al.*, 1984; Torstenfelt *et al.*, 1988; Triay *et al.*, 1993) exception the study of

(Ohe *et al.*, 1993) that has a drastic increasing sorption at all studied values of pH (from 2 to 12). In addition, the sorption in the studies of (Kozai, 1994; Sakamoto *et al.*, 1990) tends to increase by decrease pH from 5 to 2 and then starts to increase when pH is greater than 5. The increasing behavior with decreasing pH is explained by the high ion exchange between  $\text{NpO}_2^+$  in the solution and the interlayer cation  $\text{Na}^+$  which is abundant in the clay (Na-smectite). The increasing sorption with decreasing pH from 5 to 2 is also observed in (Kozai *et al.*, 1993) as a result of the expansion in the interlayer.

One can note that our sorption results were simulated under a  $\text{CO}_2$  free situation i.e. no pressure is considered. For experiments which were conducted with atmospheric pressure ( $P_{\text{CO}_2} = 10^{-3.5}$  atm), their retention behavior has a peak at pH = 8-8.5, and decreases either in acidic or in alkaline solution up to pH value of 9.5 (Turner *et al.*, 1998; Bertetti *et al.*, 1998; Bertetti *et al.*, 1995). In those studies, the decreasing in the sorption of Np(V) when  $\text{pH} \geq 8.5$  is due to the complexation of Np(V) by the carbonate in the solution.

The different trends of sorption coefficient at some ranges of pH particularly for  $\text{pH} < 7$  between the current study and the previously mentioned ones refer to the method used for sorption. Monte Carlo simulation considers all the radionuclides have (+5) valency similar neglecting the chemical and physical properties of the studied element. For example, Np(V) reduces slowly to the Np(IV) on the mineral surface in the presence of a reductant mineral such as Fe(II) and Mn(II). These minerals



are released throughout the dissolution of clays e.g. smectite. The positive sorption of Np(V) with decrease of pH from 5 to 2 observed in Kozai study (Kozai *et al.*, 1993) is demonstrated by the reduction of Np(V) to the stronger sorbing Np(IV) as a result of dissolution of smectite at lower pH (Zavarin *et al.*, 2012). Besides, in our study the radius of the ion is neglected.

Moreover, Monte Carlo simulation deals with only ion exchange mechanism to control the sorption at different ranges of pH. However, surface complexation mechanism controls the sorption of Pu(V) on montmorillonite at high pH while ion exchange controls the sorption at low pH (Zavarin *et al.*, 2012).

#### **4.4 Effect of Temperature**

The effect of temperature on the sorption process of pentavalent cations on bentonite was studied by changing the temperature from 298 to 334 K at fixed values of surface charge densities ( $-0.7$ ,  $-3$  and  $-4$  e/nm<sup>2</sup>). The simulations were performed with two bulk systems of 1 mM NaCl, 4 mM CaCl<sub>2</sub> (ground water) and 100 mM NaCl, 10 mM CaCl<sub>2</sub> (sea water) in addition to a constant amount of 1 and 0.1 mM of pentavalent cations concentration. Seven temperature values; 298, 304, 310, 322, 328 and 334 K were chosen.

Pentavalent cations concentration in electrical double layer decreases very slowly in a rate of 0.001 (Molarity/Kelvin) with increasing temperature for higher surface charge densities ( $\sigma = -3$  and  $-4$  e/nm<sup>2</sup>) as clarified in Figure 4.11. Besides, for  $\sigma = -0.7$  e/nm<sup>2</sup>, the rate of decrease in average EDL

content of  $M^{5+}$  is of order  $10^{-4}$  (M/K). It means that the temperature doesn't affect the sorption significantly. However, the decreasing of temperature could enhance the sorption process.

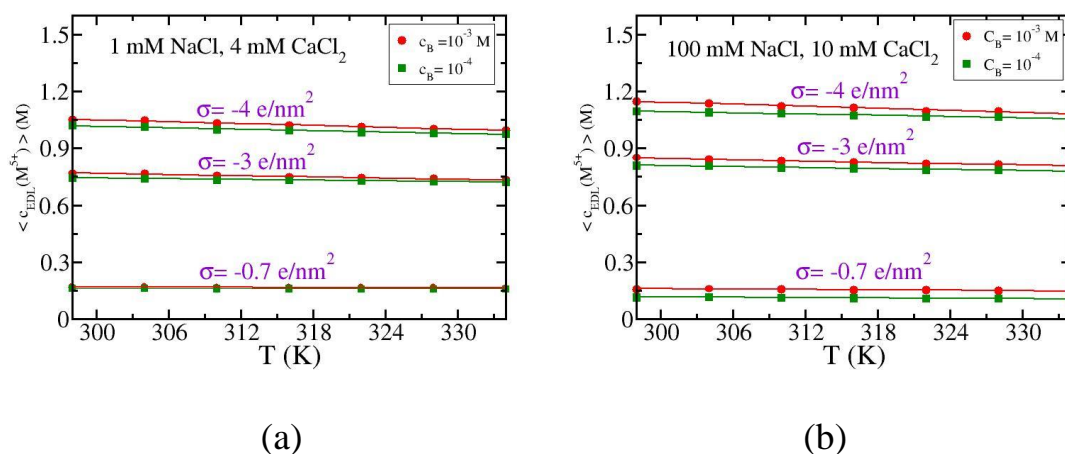


**Figure 4.11** Average electrical double layer concentration of the pentavalent cations as a function of temperature. The slit is in equilibrium with a bulk including a) 1 mM NaCl, 4 mM  $\text{CaCl}_2$  b) 100 mM NaCl, 10 mM  $\text{CaCl}_2$ . The surface charge density and the pentavalent cations concentration have been varied as pointed in the graphs. The slit width is 3 nm. The solid curves are linear fitting, while the dots are simulated results.

The results of retention coefficient as a function of temperature are summarized in Figure 4.12. Clearly, the retention coefficient reduces very slightly in a rate of order  $10^{-4}$  (1/K) with increasing temperature, so that it can be considered as constant. This behavior is attributed to the slight decrease in the electrical double layer concentration as the temperature increases.

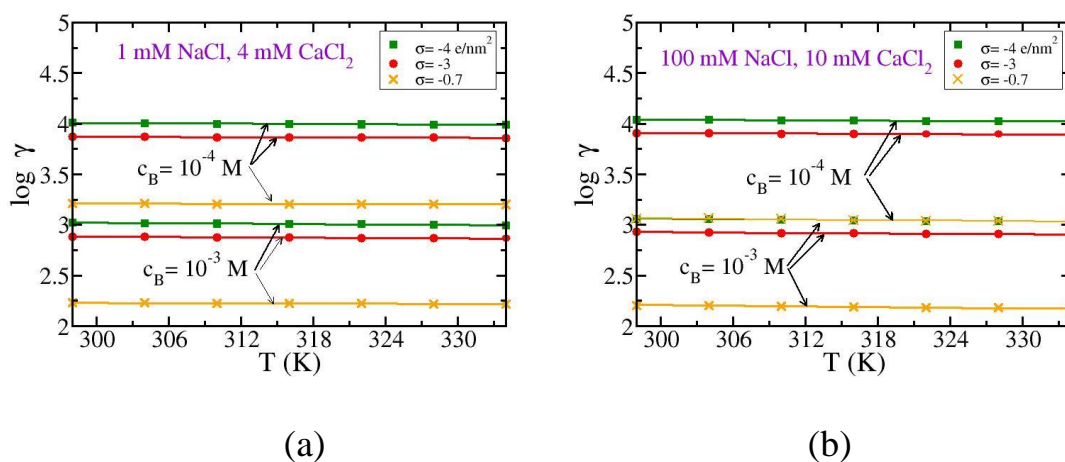


**Figure 4.12** The retention coefficient calculated from the data in Figure 4.11. The solid curves are linear fitting, while the dots are simulated results.

The decreasing in the sorption of pentavalent cations according to the increasing in the temperature could be explicated by that the sorption process of the cations is spontaneously exothermic. Moreover, one can remark from Figure 4.12 that by increasing the temperature, the retention coefficient is enhanced by:

- (a) Decreasing the pentavalent cations concentration in the bulk.
- (b) Increasing the magnitudes of surface charge density.

This is in agreement with the obtained results in sections 4.2 and 4.3, respectively.

The effect of temperature on the concentration of pentavalent cations is plotted in a different manner in Figure 4.13. It is obvious that the concentration of pentavalent cations in the double layer at small distance from the charged surface is decreasing by increasing the temperature otherwise, at large distances, the effect is less pronounced. However, the decrease rate from one curve to another is not of important effect.

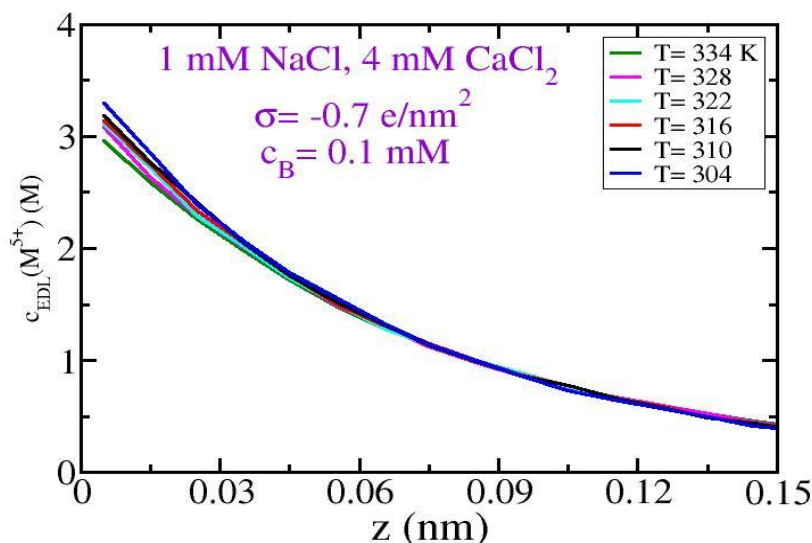


**Figure 4.13** Pentavalent cations distribution as a function of distance  $z$  outside the charged surface. The bulk solution contains 1 mM NaCl, 4 mM CaCl<sub>2</sub> and 0.1 mM of pentavalent cations. The temperature has been varied as pointed in the graph at surface charge density of  $-0.7 \text{ e/nm}^2$ . The slit width is 3 nm.

By looking to similar studies, a good agreement was found with the sorption behavior of As(V) (Zahra *et al.*, 2009). The decreasing adsorption of As(V) with increasing the temperature is presumably caused by breaking the forces which make the clay absorb the ions. While, the sorption trend of Np(V) (Ohe *et al.*, 1993) which is pointed out in Figure 4.10, Np(V) and Pu(V) (Runde *et al.*, 2002), Pu(V) (Lu *et al.*, 2009) and Sb(V) (Xi *et al.*, 2011) increases by increasing temperature. Since the adsorption process of the mentioned radioactive metals is endothermic and Monte Carlo method does not take this into considerations.

## **4.5 Effect of Solution Ionic Strength**

Monte Carlo simulations were run out to examine the sorption of pentavalent cations from different ionic strength saline solutions on bentonite clay. That is, from different kinds of water. The first part of this section (section 4.5.1) deals with solutions having fixed NaCl concentrations but variable CaCl<sub>2</sub> concentrations. While the other part (section 4.5.2) deals with solutions having variable NaCl concentrations and constant CaCl<sub>2</sub> concentrations.

### **4.5.1 Effect of Divalent Ionic Strength**

The sorption of pentavalent cations from different bulk solutions has been studied. These bulk solutions have a fixed NaCl concentration and a varied amount of CaCl<sub>2</sub> concentration. In this section, the fraction of Na<sup>+</sup>, Ca<sup>2+</sup> and M<sup>5+</sup> in the electrical double layer has been plotted at different parameters as a function of pentavalent cations concentration in the bulk. In addition, the average electrical double layer and the retention coefficient have been studied as a function of CaCl<sub>2</sub> concentration and as a function of pentavalent cations in the bulk solution. With the slit width of 3 nm, the simulations were carried out at room temperature (298 K) for two different surface charge densities (-3 and -4 e/nm<sup>2</sup>).

The fraction results of different counterions in the electrical double layer were recapped in Figure 4.14. Figure 4.14a shows the fraction in the bulk solutions of 1 mM NaCl and the CaCl<sub>2</sub> concentration has been increased from 100 to 200 and to 300 mM. While Figure 4.14b shows the fraction in

the bulk solutions including 100 mM NaCl and the amount of CaCl<sub>2</sub> has been varied from 100 to 200 and to 400 mM.

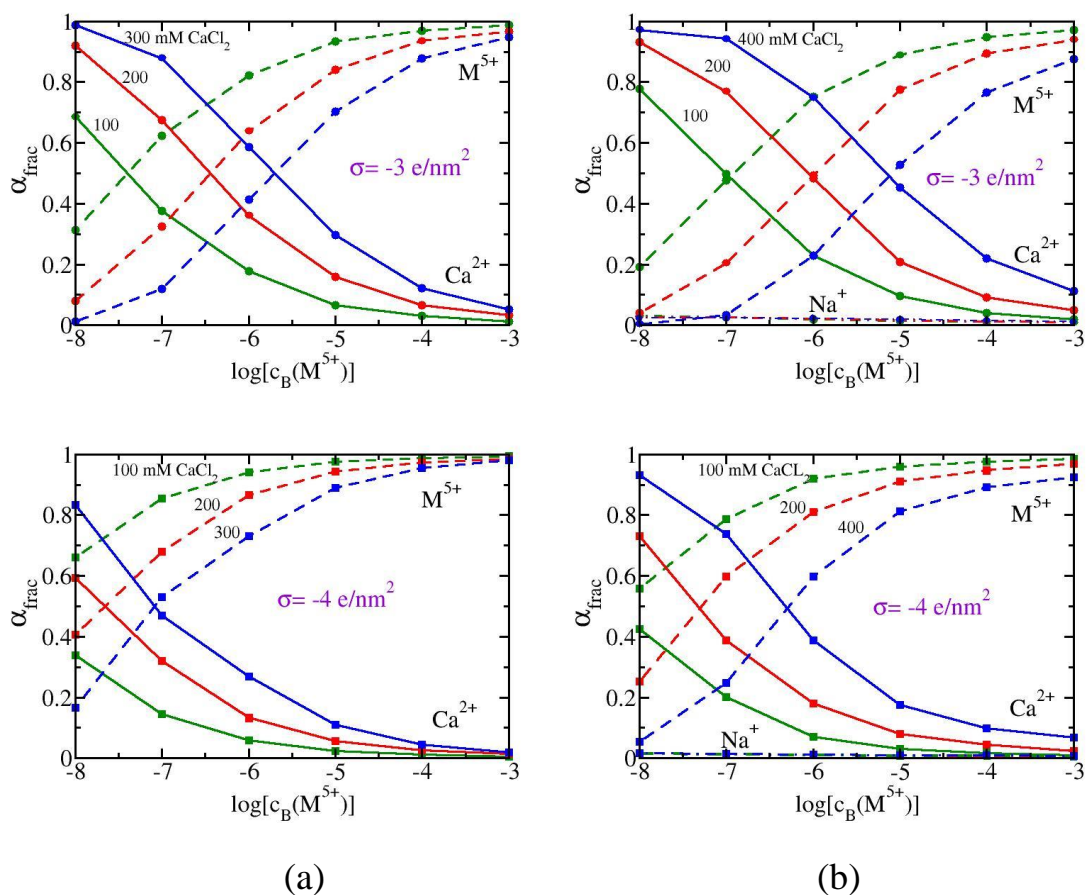


**Figure 4.14** Fraction of different counterions in the slit as a function of pentavalent cations concentration in the bulk solution. The surface charge density has been kept constant as pointed in the plots. But the bulk conditions have been varied; a) 1 mM NaCl, X mM CaCl<sub>2</sub> b) 100 mM NaCl, X mM CaCl<sub>2</sub>. The slit width is 3 nm. The values of X are obvious in the graphs.

Figure 4.14a indicates that, at  $\sigma = -3$  and  $-4$  e/nm<sup>2</sup> the fraction of pentavalent cations decreases by increasing the CaCl<sub>2</sub> concentration while the fraction of Ca<sup>2+</sup> increases by increasing the concentration of CaCl<sub>2</sub>. It is

good to note that, the fraction of monovalent species doesn't appear in the graphs since its concentration in the bulk solution is very small (1 mM).

To illustrate the behavior of fraction numerically, at specific bulk concentration of  $10^{-5}$  M of pentavalent cations and at  $\sigma = -3$  e/nm<sup>2</sup> the fractions of Ca<sup>2+</sup> and M<sup>5+</sup> are 0.0656 and 0.9343 at 1 mM NaCl, 100 mM CaCl<sub>2</sub>, respectively (Figure 4.14a). By increasing the CaCl<sub>2</sub> concentration to 200 mM the fractions of Ca<sup>2+</sup> and M<sup>5+</sup> are 0.1588 and 0.8410, respectively. While their fractions equal to 0.2976 and 0.7022 at 300 mM of CaCl<sub>2</sub>.

By looking at Figure 4.14b, the same behavior is found as in Figure 4.14a. However, in Figure 4.14b the concentration of monovalent cation appears in plots but in a low amount. Since its concentration in the three bulk solutions is small (100 mM). For example, at  $10^{-5}$  M of pentavalent cations and at  $\sigma = -3$  e/nm<sup>2</sup>, the fractions of Na<sup>+</sup>, Ca<sup>2+</sup> and M<sup>5+</sup> are 0.0145, 0.0968 and 0.8887 at 100 mM CaCl<sub>2</sub>, respectively (Figure 4.14b). While by increasing the CaCl<sub>2</sub> concentration to 400 mM, their fraction values become 0.0187, 0.4532 and 0.5281, respectively.

Interestingly, the lowest used value of CaCl<sub>2</sub> concentration (100 mM) from the different bulk solutions is the better choice to do the sorption using it. That is, 1 mM NaCl, 100 mM CaCl<sub>2</sub> (Figure 4.14a) and 100 mM NaCl, 100 mM CaCl<sub>2</sub> (Figure 4.14b) are more effective than the others to get more M<sup>5+</sup> cations in the EDL. In addition, the fraction of M<sup>5+</sup> cation at  $\sigma = -4$  e/nm<sup>2</sup> is higher than at  $\sigma = -3$  e/nm<sup>2</sup> at the same bulk conditions. In summary, the M<sup>5+</sup> cation gets more dominant at:

- 1) Lower  $\text{Ca}^{2+}$  and  $\text{Na}^+$  concentrations.
- 2) Higher  $\text{M}^{5+}$  concentrations.
- 3) Higher surface charge density.

The influence of changing the divalent cations concentration in the bulk solution on the sorption process of  $\text{M}^{5+}$  cations has been also investigated by direct calculation of the average EDL concentration and the retention coefficient. Figure 4.15 represents the average electrical double layer as a function of  $\text{CaCl}_2$  concentration. In addition to  $\text{CaCl}_2$ , the bulk includes 1 mM NaCl (4.15a), 100 mM NaCl (4.15b) and 0.00001 mM of  $\text{M}^{5+}$  cations.

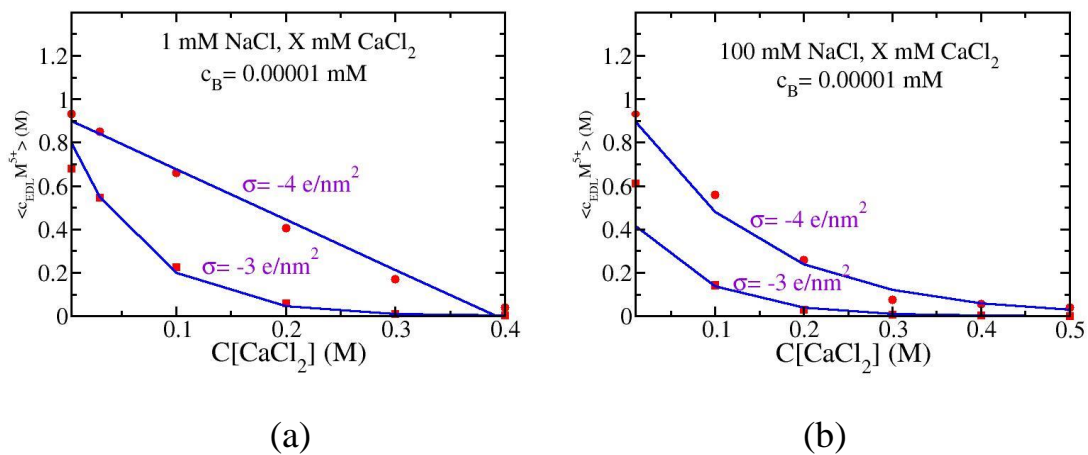


**Figure 4.15** Average electrical double layer concentration of pentavalent cations as a function of  $\text{CaCl}_2$  concentration at surface charge densities of  $-3$  and  $-4 \text{ e/nm}^2$ . The bulk includes a) 1 mM NaCl, X mM  $\text{CaCl}_2$  b) 100 mM NaCl, X mM  $\text{CaCl}_2$  and 0.00001 mM of pentavalent cations. The solid curves are linear or exponential fitting, while the dots are simulated results.

The concentration of  $\text{CaCl}_2$  is varied up to 400 mM (Figure 4.15a) and up to 500 mM (Figure 4.15b). The results reveal that the concentration of



pentavalent cations gets more abundant in the electrical double layer by decreasing the  $\text{CaCl}_2$  concentration.

Moreover, the retention coefficient calculated from data in Figure 4.15 tends to decrease by increasing the concentration of divalent cations in the bulk solution as shown in Figure 4.16. This means that the salinity of the solution retards the sorption of pentavalent cations from the solution.

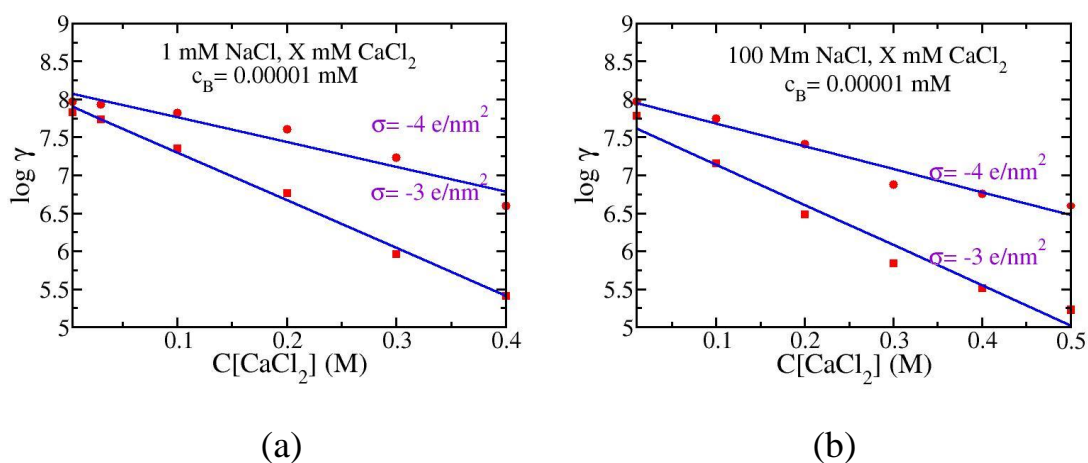


**Figure 4.16** The retention coefficient calculated from the data in Figure 4.15. The solid curves are linear fitting, while the dots are simulated results.

The reduction of the sorption of radioactive metals by increasing the ionic strength of the solution can be elucidated by the presence of many counterions resulted from the additive amount of the salt ( $\text{CaCl}_2$ ) to the bulk solution. These additional cations lead to high competition for the charged surface. For this reason, the probability of sorption of pentavalent cations will decrease.

The concentration of counterions in the electrical double layer as a function of nanometric distance  $z$  at different bulk solutions is demonstrated in

Figure 4.17. Such solutions have the same NaCl concentration (1mM) but variable amount of CaCl<sub>2</sub>. The surface charge density is  $-4 \text{ e/nm}^2$ . For example, an increase of the CaCl<sub>2</sub> concentration from 30 mM (blue curves) to 300 mM (green curves) leads to a significant decrease of M<sup>5+</sup> distribution. Accordingly, there will be an increase in Ca<sup>2+</sup> distribution. This demonstrates again the impact of salinity on the cations concentration in the double layer, and also illustrates the replacement of M<sup>5+</sup> by Ca<sup>2+</sup> in the interlayer.

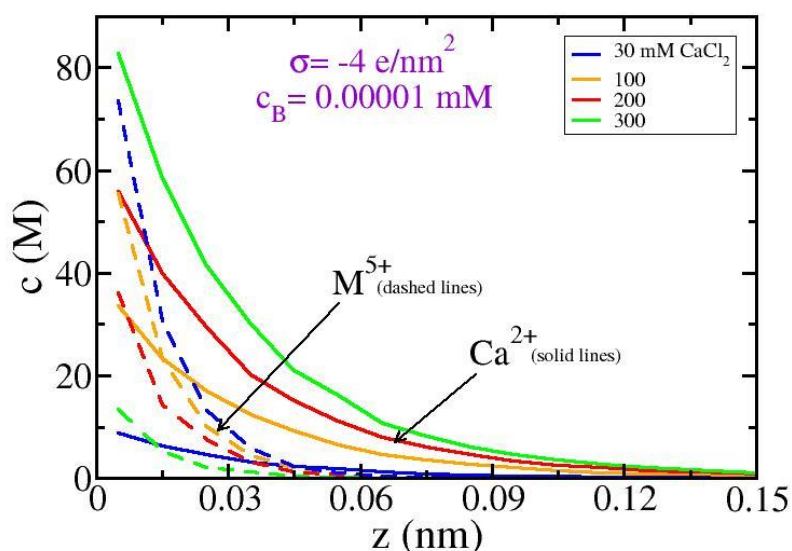


**Figure 4.17** Counterion distribution as a function of distance  $z$  outside the charged surface. Different bulk solutions are shown with 1 mM NaCl and varied amount of CaCl<sub>2</sub> concentration. The surface charge density is  $-4 \text{ e/nm}^2$  and the pentavalent cations concentration is 0.00001 mM.

The average EDL concentration of pentavalent cations as a function of their concentration in the bulk solutions of various amount of CaCl<sub>2</sub> is shown in Figure 4.18. Obviously, decreasing CaCl<sub>2</sub> concentration in the bulk will

enhance the sorption process. Accordingly, the 100 mM  $\text{CaCl}_2$  is the effective divalent concentration from the others. In addition, at higher pentavalent concentration the average concentration diverges to a certain value for each  $\sigma$ , and is getting independent of  $\text{CaCl}_2$  concentration.

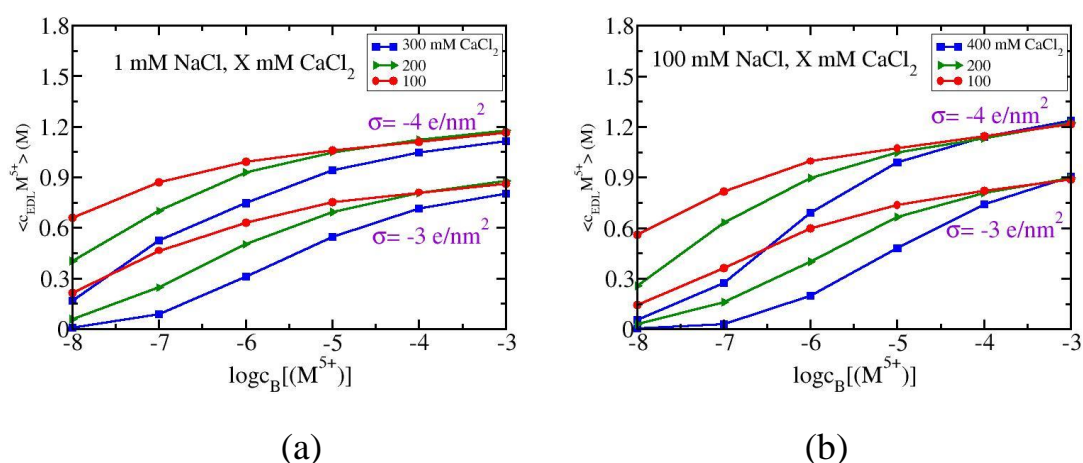


**Figure 4.18** Average electrical double layer concentration of pentavalent cations as a function of their bulk concentration. The bulk conditions have been varied; a) 1 mM NaCl, X mM  $\text{CaCl}_2$  b) 100 mM NaCl, X mM  $\text{CaCl}_2$  at surface charge density of  $-3$  and  $-4 \text{ e/nm}^2$ . The slit width is 3 nm.

The retention coefficient of pentavalent cations according to their bulk concentration for different kinds of water is displayed in Figure 4.19. The results emphasize that, the sorption decreases by increasing the divalent cations concentration especially at low pentavalent concentration. However, this effect is getting less important at higher  $M^{5+}$  concentration. In addition, the sorption decreases as the amount of  $M^{5+}$  cations increases.

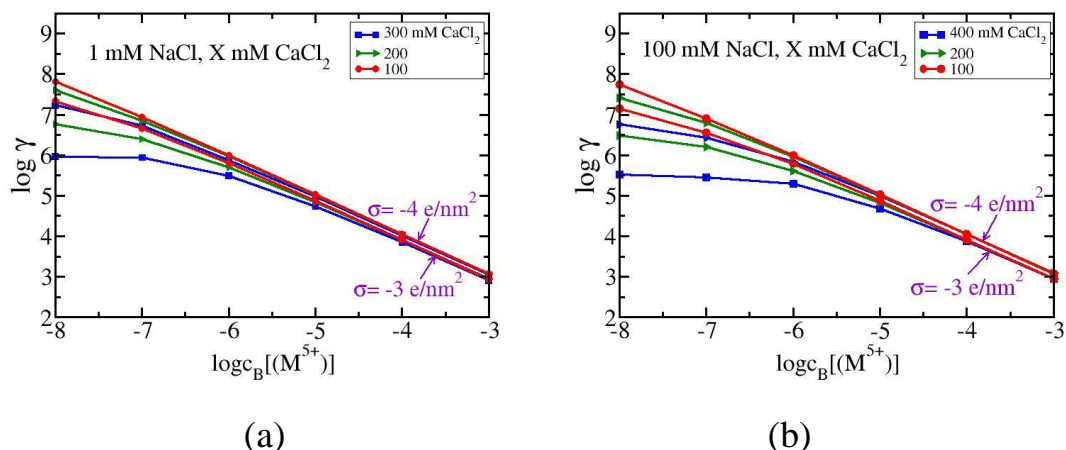


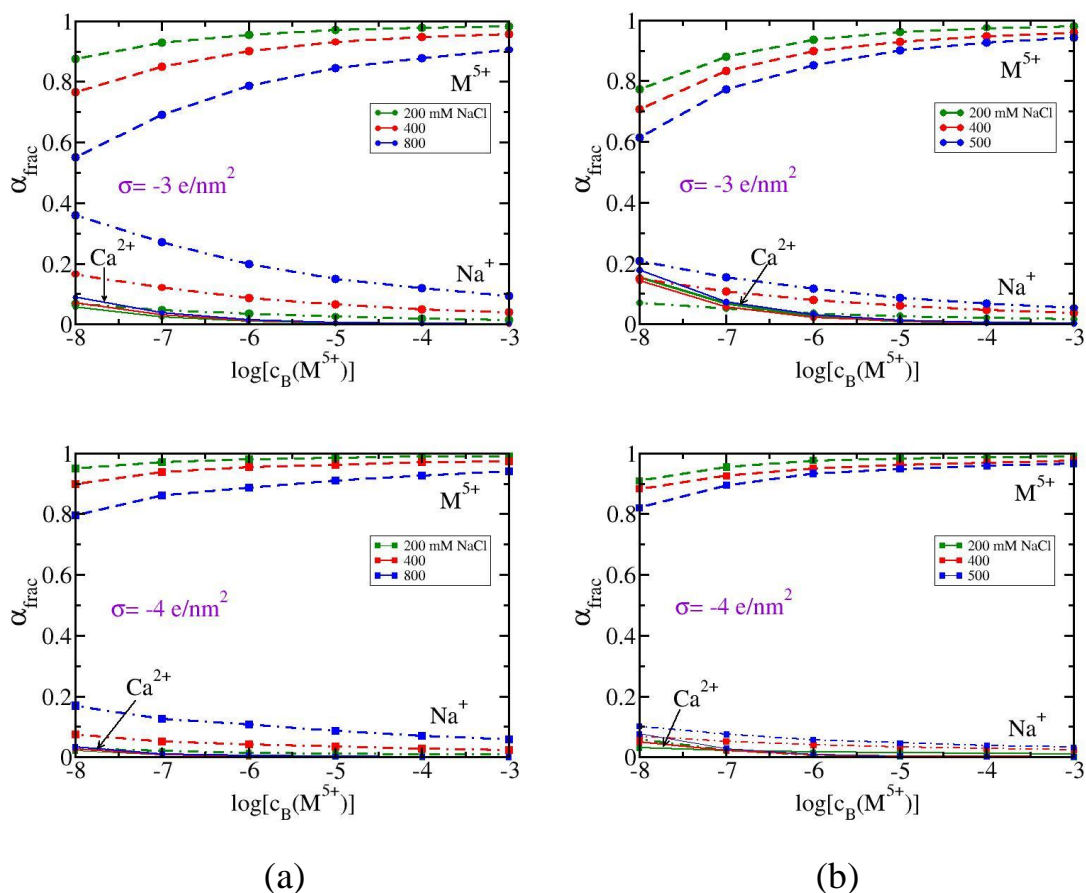
**Figure 4.19** The retention coefficient calculated from the curves in Figure 4.18.

Our obtained results agree with the experimental study of (Zavarin *et al.*, 2013), in which the sorption of Np(V) increased by decreasing the  $\text{CaCl}_2$  concentration from (0.1 to 0.01 and to 0.001 M). They also agree with the work of (Kozai *et al.*, 1994) which demonstrates that when the exchangeable cation included in bentonite ( $\text{Ca}^{2+}$ ) released to the solution, the sorption of Np(V) reduced. Moreover, the adsorption process of Pu(V) was found to be decreased by increasing the ionic strength of the solution (Lu *et al.*, 2009).

### 3.5.2 Effect of Monovalent Ionic Strength

Additional simulations were done to investigate the effect of ionic strength on the sorption process on bentonite clay by varying the concentration of NaCl, while the concentration of  $\text{CaCl}_2$  was fixed. In this section, the fraction of different cations in the electrical double layer has been studied as a function of pentavalent cations in the bulk. Furthermore, the average double layer concentration and the retention coefficient were plotted as a function of NaCl concentration. The simulations were run at room

temperature (298 K) and at surface charge densities of  $-3$  and  $-4$   $\text{e}/\text{nm}^2$ . The fraction of  $\text{Na}^+$ ,  $\text{Ca}^{2+}$  and  $\text{M}^{5+}$  as a function of  $\text{M}^{5+}$  cations concentration at different bulk conditions is shown in Figure 4.20.



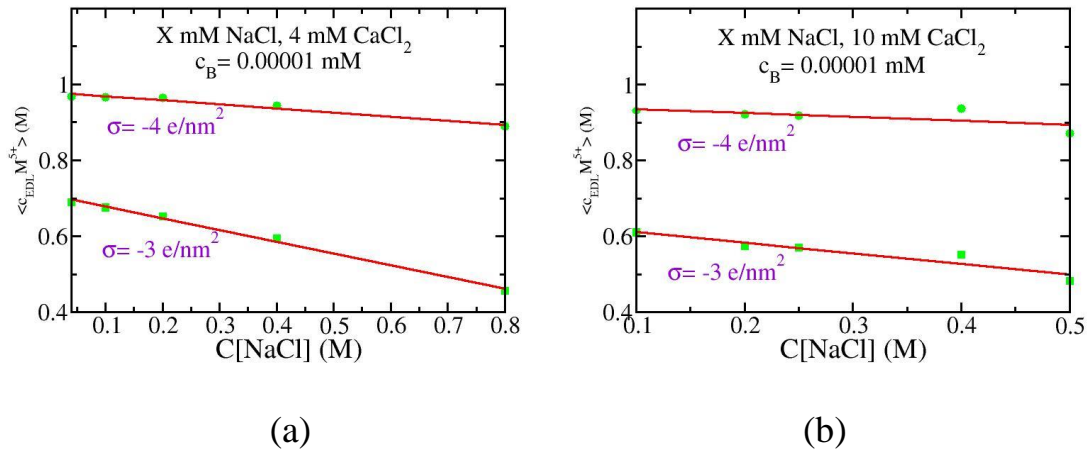
**Figure 4.20** Fraction of different counterions in the slit as a function of pentavalent cations concentration in the bulk solution. The surface charge density has been kept constant as pointed in the plots. While the bulk conditions have been varied; a) X mM NaCl, 4 mM  $\text{CaCl}_2$  b) X mM NaCl, 10 mM  $\text{CaCl}_2$ . The slit width is 3 nm. The values of X are obvious in the graphs.

Figure 4.20a presents the fraction in bulk solutions of 4 mM  $\text{CaCl}_2$  and the NaCl concentration is increased from 200 to 400 and to 800 mM, while the

fraction in bulk solutions of 10 mM  $\text{CaCl}_2$  and the NaCl amount is varied from 200 to 400 and to 500 mM is illustrated in Figure 4.20b.

The obtained results at surface charge densities of  $-3 \text{ e/nm}^2$  and  $-4 \text{ e/nm}^2$  indicate that by increasing the concentration of NaCl in the bulk solution, the fraction of pentavalent cation decreases significantly. While the fraction of monovalent cation increases clearly but the fraction of divalent cation increases very slowly since its concentration in the bulk is very small. Note that, the fraction of  $\text{M}^{5+}$  completely dominates over  $\text{Na}^+$  and  $\text{Ca}^{2+}$  species.

For example, Figure 4.20a illustrates that, at  $\sigma = -3 \text{ e/nm}^2$  and at  $10^{-6} \text{ M}$  of pentavalent cations, the fractions of  $\text{Na}^+$ ,  $\text{Ca}^{2+}$  and  $\text{M}^{5+}$  are 0.1987, 0.0142 and 0.7871, respectively at bulk solution of 800 mM NaCl, 4 mM  $\text{CaCl}_2$ . By lowering the NaCl concentration to 400 mM, the fraction of  $\text{Na}^+$ ,  $\text{Ca}^{2+}$  and  $\text{M}^{5+}$  will be 0.0878, 0.0117 and 0.9007, respectively. One can conclude that, the lowest used concentration of NaCl (200 mM) is more effective than other concentrations to adsorb more pentavalent pollutants on the clay. Moreover, the increased sorption trend with decreasing monovalent cations concentration in the bulk solution is also investigated by studying the average EDL concentration by varying the amount of NaCl concentration (Figure 4.21). In Figure 4.21a, it is obvious that by increasing the NaCl up to 800 mM at surface charge densities of  $-3$  and  $-4 \text{ e/nm}^2$  with  $10^{-5} \text{ mM}$  of pentavalent cations, the average electrical double layer concentration tends to decrease. The same behavior was found in Figure 4.21b, when the concentration of monovalent cation is changed from 100 to 500 mM.



**Figure 4.21** Average electrical double layer concentration of pentavalent cations as a function of NaCl concentration at surface charge densities of -3 and -4  $e/nm^2$ . The bulk includes a) X mM NaCl, 4 mM  $CaCl_2$  b) X mM NaCl, 10 mM  $CaCl_2$  and 0.00001 mM of pentavalent cations. The solid curves are linear fitting, while the dots are simulated results.

Furthermore, the retention coefficient of pentavalent cations as a function of NaCl concentration at  $10^{-5}$  mM of pentavalent cations is clarified in Figure 4.22. It reduces by increasing the concentration of NaCl. The decreasing in the retention coefficient of  $M^{5+}$  with increasing the monovalent cations in the bulk is imputed to high competition of counterions on the charged surface. That competition resulted from the additional amount of NaCl concentration in the solutions. Therefore, the possibility of adsorption  $M^{5+}$  cations is becoming less.

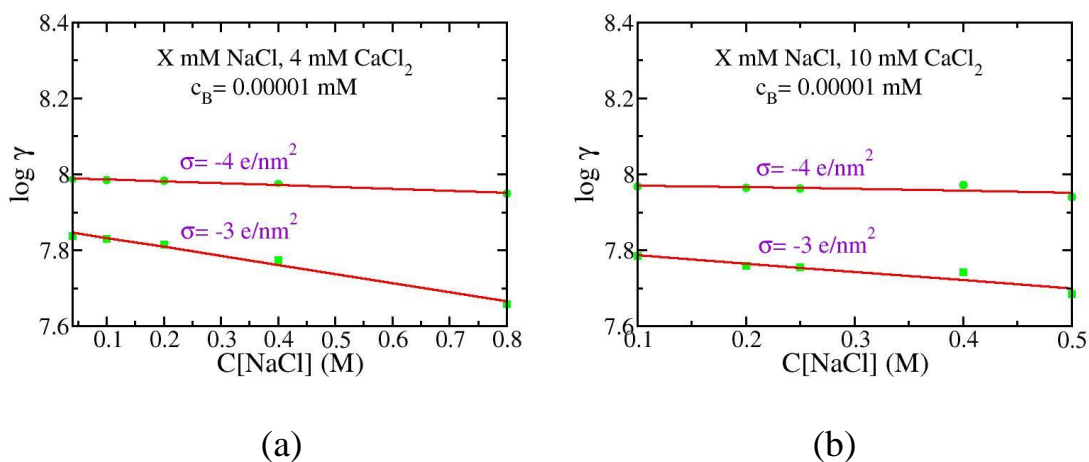


**Figure 4.22** The retention coefficient calculated from the data in Figure 4.21. The solid curves are linear fitting, while the dots are simulated results.

The spatial distribution of different counterions is demonstrated in Figure 4.23 at surface charge density of  $-4 \text{ e/nm}^2$  with  $10^{-5}$  mM of pentavalent cations. It is clear that, by increasing the NaCl concentration from 400 to 800 mM (Figure 4.23a) and from 200 to 500 mM (Figure 4.23b), the distribution of pentavalent cations decreased, while the mono- and divalent distributions increased.

Note that, the divalent cations distribution is not affected compared to monovalent ones. Since at different bulk solutions, the  $\text{CaCl}_2$  is fixed and small; 4 mM (4.23 a) and 10 mM (4.23 b). In addition, monovalent species are dominant over divalent ones (Figure 4.23 a) however the divalent species are dominant over monovalent ones (Figure 3.23 b). This is presumably due to the  $\text{CaCl}_2$  concentration which in (4.23 a) is less than in (4.23 b).



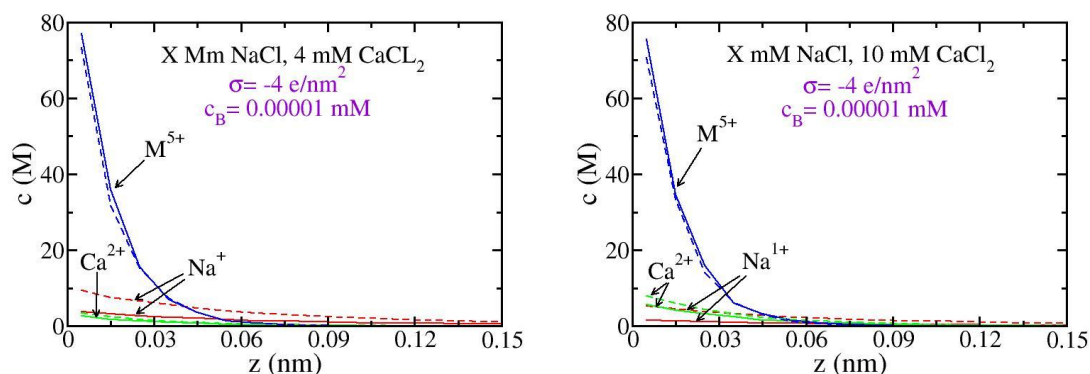


**Figure 4.23** Counterion distribution as a function of distance  $z$  outside the charged surface. Two different bulk systems are shown with a) 400 mM NaCl, 4 mM  $\text{CaCl}_2$  (solid lines) and 800 mM NaCl, 4 mM  $\text{CaCl}_2$  (dashed lines) b) 200 mM NaCl, 10 mM  $\text{CaCl}_2$  (solid lines) and 500 mM NaCl, 10 mM  $\text{CaCl}_2$  (dashed lines). The slit width is 3 nm.

The results of ionic strength are in agreement with the related experimental studies. For example, the work of (Zavarin *et al.*, 2012) shows a decreasing trend of Np(V) and Pu(V) sorption by increasing the NaCl concentration. Also this behavior was found in the sorption of Np(V) by varying the ionic strength of NaCl and KCl (Zavarin *et al.*, 2013). Besides, the study of (Sabodina *et al.*, 2006) displays a decreasing behavior by increasing the ionic strength from (0.1 to 0.01 and to 0.001 M) which is maintained by  $\text{NaClO}_4$  at low values of pH.

Finally, the volume of the influence of varying the amount of mono- and divalent cations in the solution is clear in Figure 4.24. By comparing the rate of decrease shown in the plots, the effect of changing the ionic strength at specific  $\text{M}^{5+}$  concentration ( $10^{-5}$  mM) and at  $\sigma = -3$  e/nm<sup>2</sup> is more obvious in the simulations that changed the divalent cations concentration

(Figure 4.24b). That is, increasing the ionic strength which is maintained by divalent cations will impact the retention coefficient more than the monovalent ones. Moreover, the decreasing rate in the blue curves is higher than in the red ones.

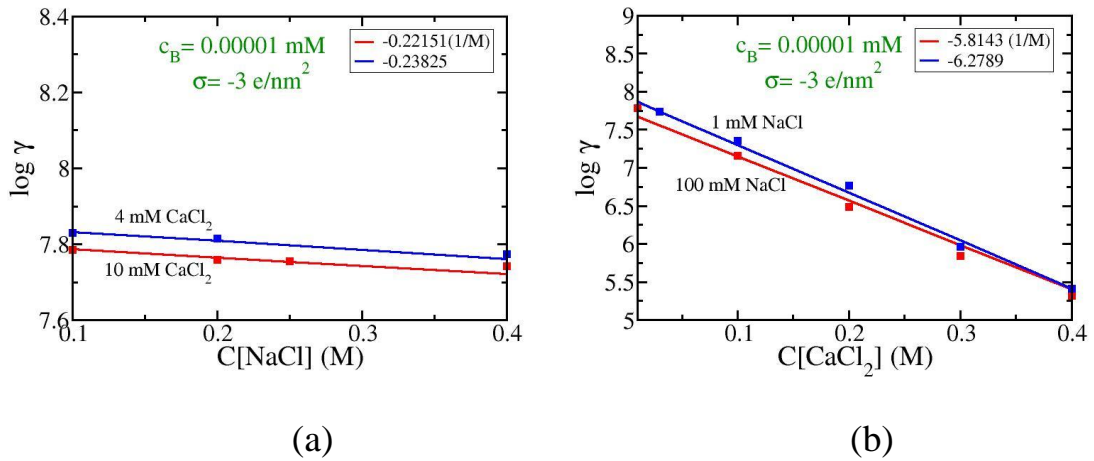


**Figure 4.24** The retention coefficient of pentavalent cations as a function of a) NaCl b)  $\text{CaCl}_2$  concentration at surface charge density of  $-3 \text{ e/nm}^2$  with  $10^{-5} \text{ mM}$  of  $\text{M}^{5+}$  cations. The decreasing rate of the curves is indicated in the plots. The solid curves are linear fitting, while the dots are simulated results.

## Chapter Five

### Conclusions

Monte Carlo simulations have been used in grand canonical ensemble to generate numerical results for the sorption process of pentavalent ions on bentonite using the primitive model of NaCl and CaCl<sub>2</sub> electrolytes next to planer uniformly charged walls. The simulations were carried out for negative surface charge densities over pentavalent bulk concentration ranging from 10<sup>-8</sup> to 10<sup>-3</sup> (M). Based on the obtained results, the following can be concluded:

- (1) The sorption process of pentavalent cations on bentonite clay is affected by the concentration of M<sup>5+</sup> in the bulk, the surface charge density over the walls, the temperature of the system and the ionic strength of the solution.
- (2) The average electrical double layer concentration of M<sup>5+</sup> pollutants is:
  - a) Increasing by increasing the pentavalent concentration in the bulk and the surface charge density.
  - b) Decreasing by increasing the ionic strength of mono- and divalent cations.
  - c) Decreasing slowly by increasing the temperature.
- (3) The retention coefficient of M<sup>5+</sup> pollutants tends to:
  - a) Increase by increasing the surface charge density.
  - b) Decrease by increasing the pentavalent concentration in the bulk and the ionic strength of mono- and divalent cations.

- c) Decrease slightly by increasing temperature.
- (4) The fraction of  $M^{5+}$  cations increases as a function of their bulk concentration, while the fraction of  $Ca^{2+}$  and  $Na^+$  decreases. In addition, the fraction of  $M^{5+}$  species gets more abundant at higher values of surface charge density, higher concentrations of pentavalent cations in the bulk and lower  $Ca^{2+}$  and  $Na^+$  concentrations.
- (5) The spatial distribution (concentration) of pentavalent cations in the electrical double layer is decreasing exponentially with increasing the distance from the charged surface.
- (6) The results also assert that, the bentonite clay is an effective material for retention, immobilization and removal of pentavalent radionuclides from huge volumes of waste water. Moreover, Monte Carlo is an effective, accurate and economical method to investigate the sorption process on clays.

## References

- Allard B., Olofsson U., and Torstenfelt B., "**Environmental actinide chemistry**", *Inorganic ChimicaActa*, **94**(4), 205-221(1984).
- Allen M. P., and Tildesley D. J., "**Computer simulation of liquids**", Clarendon Press, Oxford, (1987).
- Bardbury M. H., and Baeyens B., "**Modelling the sorption of Mn(II), Co(II), Ni(II), Zn(II), Cd(II), Eu(III), Am(III), Sn(IV), Th(IV), Np(V), U(VI) on montmorillonite: linear free energy relationships and estimates of surface binding constants for some selected heavy metals and actinides**", *Geochimica et CosmochimicaActa*, **69**(4), 875-892(2005).
- Bartl U., and Czurda K.A., "**Migration and retention phenomena of radionuclides in clay-barrier systems**", *Applied Clay Science*, **6**, 195-214(1991).
- Beall G. W., and Allard B., "**Sorption of actinides from aqueous solutions under environmental conditions**". In: Tewari P. H., editor, "**Adsorption from aqueous solutions**", Springer US, 193-212(1981).
- Begg J. D., Zavarin M., Zhao P., Tumey S. J., Powell B., and Kersting A. B., "**Pu(V) and Pu(IV) sorption to montmorillonite**", *Environ. Sci. Technol.*, **47**, 5146-5153(2013).
- Beichl I., and Sullivan F., "**The Metropolis algorithm**", *Computing in Science and Engineering*, **2**, 65-69(2000).
- Bertetti F. P., Pabalan R. T., and Almendarez M. G., "**Studies of neptunium(V) sorption on quartz, clinoptilolite, montmorillonite,**

- and  $\alpha$ -alumina"**. In: Jenne E. A., editor, "**Adsorption of metals by geomedia: variables, mechanisms, and model variations**", Academic Press, New York, 131-148(1998).
- Bertetti F. P., Pickett D. A., and Pabalan R. T., "**Sorption modeling for high-level waste performance assessment**". In: Saqar B., editor, "**NRC high-level radioactive waste research at CNWRA**", CNWRA report 95-01 S, San Antonio, Texas, (1995).
  - Butt H. J., Graf K., and Kappl M., "**Physics and chemistry of interfaces**", WILEY-VCH Verlag GmbH & Co. KGaA, Weinheim, (2003).
  - Chutia P., Kato S., Kojima T., and Satokawa S., "**Arsenic adsorption from aqueous solution on synthetic zeolites**", Journal of Hazardous Materials, **162**(1), 440-447(2009).
  - Cronstrand P., "**Assesment of uncertainty intervals for sorption coefficient**", SKB rapport R-05-75, (2005).
  - Delattre-Louvel F., Lapeyre C., Struillou R., and Arnould M., "**Retention mechanisms for toxic cations using artificial confinement barriers of clay-cement mixtures**", Engineering Geology, **34**, 151-158(1993).
  - Derjaguin B., and Landau L., "Theory of the stability of strongly charged lyophobic sols and of the adhesion of strongly charged particles in solution of electrolytes", ActaPhysicochim.URSS, **14**, (1941).
  - Dongarra J., and Sullivan F., "**Guest editors' introduction: the top 10 algorithms**", Computing in Science and Engineering, **2**, 22-32(2000).

- Dzombak D. A., and Hudson R. J. M., "**Ion exchange: the contributions of diffuse layer sorption and surface complexation**". In: Hunag C. P., O'Melia C. R., and Morgan J. J., editors, "**Aquatic chemistry: interfacial and interspecies process**", American Chemical Society, Washington DC, (1995).
- Elam M., and Sundqvist G., "**Meddling in the KBS programme and Swedish success in nuclear waste management**", Paper prepared for the conference Managing Radioactive Waste: Problems and Challenges in a Globalizing World, University of Gothenburg, Sweden, (2009).
- Endo T., Yamamoto S., Honna T., and Eneji A. E., "**Sodium-calcium exchange selectivity as influenced by clay minerals and composition**", Soil Science, **167**(2), 117-125(2002).
- Eylem C., Erten H. N., and Gokturk H., "**Sorption of barium on kaolinite, montmorillonite and chlorite**", Analyst, **114**(3), 351-353(1989).
- Faure G., "**Principles and applications of geochemistry**", 2<sup>nd</sup> Ed, Prentice-Hall, Inc., New Jersey, (1998).
- Fletcher P., and Sposito G., "**The chemical modeling of clay/electrolyte interactions for montmorillonite**", Clay Minerals, **24**, 375-391(1989).
- Frenkel D., and Smit B., "**Understanding molecular simulation: from algorithms to applications**", Academic Press, San Diego, (1996).
- Gelman A., Roberts G. O., and Gilks W. R., "**Efficient Metropolis jumping rules**", Bayesian Statistics, **5**, 599-601(1996).

- Gera F., Pellegrini R., and Tassoni E., "**Research activities and feasibility analyses for nuclear waste disposal in clay deposits**", Regional Meeting: Nuclear Energy in Central Europe Present and Perspectives, portoroz, Solvenia, **13**(16), 482-489(1993).
- Grim R. E., "**Clay mineralogy**", 1<sup>st</sup> Ed, McGraw-Hill Book Co., New York, (1953).
- Grim R. E., "**Applied clay mineralogy**", McGraw-Hill Book Company, New York, (1962).
- Grim R. E., "**Clay mineralogy**", 2<sup>nd</sup> Ed, McGraw-Hill Book Company, New York, (1968).
- Guldbrand L., Jonsson B., Wennerstrom H., and Linse P., "**Electrical double layer forces. A Monte Carlo study**", J. Chem. Phys., **80**(5), 2221-2223(1984).
- Hansen J. P., and McDonald I. R., "**Theory of simple liquids**", 3<sup>rd</sup> Ed, Academic Press, (2006).
- Hill T. L., "**Statistical mechanics: principles and selected applications**", McGraw-Hill, New York, (1956).
- Hsu T., "**Experimental assessment of adsorption of Cu<sup>+2</sup> and Ni<sup>+2</sup> from aqueous solution by oyster shell powder**", Journal of Hazardous Materials, **171**, 995-1000(2009).
- Jeffery A., Scott E., and Donald A., "The modified Gouy-Chapman theory: comparisons between electrical double layer models of clay swelling", Languimer, 10(7), 2125-2126(1994).



- Jonsson B., Labbez C., and Cabane B., "Interaction of nanometric clay platelets", *Langmuir*, **24**, 11406-11410(2008).
- Jonsson B., Persello J., Li J ., and Cabane B., "**Equation of state of colloidal dispersions**", *Langmuir*, **9**, A-C(2011).
- Khan S. A., Rehman R., and Khan M. A., "**Adsorption of chromium(III), chromium(VI) and silver(I) on bentonite**", *Waste Management*, **15**(4), 271-282(1995).
- Kozai N., Ohnuki T., and Muraoka S., "**Sorption characteristics of neptunium by sodium-smectite**", *Journal of Nuclear Science and Technology*, **30**(11), 1153-1159(1993).
- Kozai N., "**Performance of engineered barrier materials: sorption characteristics of neptunium by smectite**", In: Muraoka S., Senoo M., Sekine K., editors, "**Progress report on safety research on radioactive waste management for the period April 1992 to March 1993**", JAERI-M94-027, Tokyo, Japan Atomic Energy Research Institute, 39-41(1994).
- Kozai N., Ohnuki T., and Muraoka S., "**Sorption behavior of neptunium on bentonite-effect of calcium ion on the sorption -**", *MRS Proceedings*, **353**, (1994).
- Li J., Hu J., Sheng G., Zhao G., and Huang Q., "**Effect of pH, ionic strength, foreign ions and temperature on the adsorption of Cu(II) from aqueous solution to GMZ bentonite**", *Colloids and Surfaces A: Physicochem. Eng. Aspects*, **349**, 195–201(2009).

- Li Y. H., Wang S., Luna Z., Ding J., Xu C., and Wu D., "**Adsorption of cadmium(II) from aqueous solution by surface oxidized carbon nanotubes**", Carbon, **41**, 1057-1062(2003).
- Lu N., Reimus P. W., Parker G. R., Conca J. L., and Triay I. R., "**Sorption kinetics and impact of temperature, ionic strength and colloid concentration on the adsorption of plutonium-239 by inorganic colloids**", RadiochimicaActa, **91**(12), 713-720(2009).
- Lujaniene G., Sapolaite J., Amulevicius A., Mazeika K., and Motiejunas S., "**Retention of cesium, plutonium and americium by engineered and natural barriers**", Czechoslovak Journal of Physics, **56**, (2006).
- Lumiste L., Munter R., Sutt J., Kivimae T., and Eensalu T., "**Removal of radionuclides from Estonian groundwater using aeration, oxidation, and filtration**", Proceeding of the Estonian Academy of Science, **61**(1), 58-64(2012).
- Maraaba I., "**Studying the retention of multivalent pollutants in bentonite**", master thesis, An-Najah National University, (2014).
- Marcus R. A., "**Titration of polyelectrolytes at higher ionic strengths**", J. Phys. Chem., **58**, 621-623(1954).
- Martin M. I., Lopez F. A., Perez C., Lopez-Delgado A., and Alguacil F. J., "**Adsorption of heavy metals from aqueous solutions with by-products of the steelmaking industry**", Journal of Chemical Technology and Biotechnology", **80**(11), 1223-1229(2005).

- McBride D. G., Prendiville P. W., and Hoover M. G., "**Design of the Los Angeles aqueduct water filtration plant**", Public Works, **113**, 36-38(1991).
- McBride M. B., "**Environmental chemistry of soils**", Oxford University Press, New York, Oxford, (1994).
- McBride M. B., "A critique of diffuse double layer models applied to colloid and surface chemistry", Clays and Clay Minerals, 45(4), 598-608(1997).
- McQuarrie D. A., "**Statistical mechanics**", 1<sup>st</sup> Ed., Harper & Row, New York, NY, (1976).
- Metropolis N. A., Rosenbluth A. W., Rosenbluth M. N., Teller A., and Teller E., "**Equation of state calculations by fast computing machines**", J. Chem. Phys., **21**, 1087-1092(1953).
- Meunier A., "**Clays**", New York: Springer, (2005).
- Mitchell J. K., "**Fundamentals of soil behavior**", John Wiley and Sons, Inc., New York, (1993).
- Norman G. E., and Filinov V. S., "**Investigations of phase transitions by a Monte Carlo method**", High Temperature, **7**(7), 216-222(1969).
- Ohe T., Tsukamoto M., Fujita T., Hesbol R., and Hermansson H. P., "**Temperature and pH dependence of neptunium(V) sorption on bentonite**", Proceedings of the 1993 International Conference on Nuclear Waste Management and Environmental Remediation, volume 1: Low and intermediate level radioactive waste management, Prague, Czechoslovakia, 197-205(1993).

- Poernomo H., "**Sorption and dispersion of strontium radionuclide in the bentonite-quartz-clay as backfill material candidate on radioactive waste repository**", Indo. J. Chem., **10**(3), 276-284(2010).
- Robert C. P., and Casella G., "**Introducing Monte Carlo method with R**", 1<sup>st</sup> Ed., Springer, New York, (2010).
- Robinson B. P., "**Ion-exchange minerals and disposal of radioactive wastes- a survey of literature**", United States Government Printing Office, Washington, (1962).
- Runde W., Conradson S. D., Efurud D. W., Lu N., VanPelt C. E., and Tait C.D., "**Solubility and sorption of redox-sensitive radionuclides (Np, Pu) in J-13 water from the Yucca Mountain site: comparison between experiment and theory**", Applied Geochemistry, **17**, 837-853(2002).
- Sabodina M. N., Kalmykov S. N., Sapozhnikov Yu. A. and Zakharova E. V., "**Neptunium, plutonium and <sup>137</sup>Cs sorption by bentonite clays and their speciation in pore waters**", Journal of Radioanalytical and Nuclear Chemistry, **270**(2), 349-355(2006).
- Sakamoto Y., Konishi M., Shirahashi k., Senoo M., Moriyama N., "**Adsorption behavior of neptunium for soil**", Radioactive Waste Management and the Nuclear Fuel Cycle, **15**, 13-25(1990).
- Segad M., Jonsson B., Akesson T., and Cabane B., "**Ca/Na montmorillonite: structure, forces and swelling properties**", Langmuir, **26**(8), 5782-5790(2010).

- Selvi K., Pattabhi S., and Kadirvelu K., "**Removal of Cr(VI) from aqueous solution by adsorption onto activated carbon**", *Bioresource technology*, **80**, 78-89(2001).
- Stumm W., "**Chemistry of the solid-water interface**", John Wiley and Sons, Inc., New York, USA, (1992).
- Torrie G. M., and Valleau J. P., "Electrical double layers. I. Monte Carlo study of a uniformly charged surface", *J. Chem. Phys.*, 73(11), 5807-5808(1980).
- Torrie G. M., and Valleau J. P., "**Electrical double layers. 4. Limitations of the Gouy-Chapman theory**", *J. Phys. Chem.*, **86**(16), 3251-3252(1982).
- Torstenfelt B., Rundberg R. S., and Mitchell A. J., "**Actinide sorption on granites and minerals as a function of pH and colloids/pseudocolloids**", *Radiochimica Acta*, **44-45**(1), 111-117(1988).
- Trauger R. J., "**The structure, properties, and analysis of bentonite in geosynthetic clay liners**", geosynthetic research institute, Philadelphia, (1994).
- Triay I. R., Robinson B. A., Lopez R. M., Mitchell A. J., and Overly C. M., "**Neptunium retardation with tuffs and groundwaters from Yucca Mountain**", Proceedings of 4<sup>th</sup> Annual International Conference on High- Level Radioactive Waste Management. La Grange Park, IL: Am Nuclear Soc, 1504-1508(1993).
- Tsezos M., and Volesky B., "**Bisorption of uranium and thorium**", *Biotechnology and Bioengineering*", **XX111**, 583-604(1981).

- Turner D. R., Pabalan R. T., and Bertetti F. B., "**Neptunium(V) sorption on montmorillonite: an experimental and surface complexation modeling study**", *Clays and Clay Minerals*, **46**(3), 256-269(1998).
- Valleau J. P., Ivkov R., and Torrie G. M., "**Colloid stability: the forces between charged surfaces in an electrolyte**", *J. Chem. Phys.*, **95**(1), (1991).
- Van Olphen H., "**An introduction to clay colloid chemistry**", 2<sup>nd</sup> Ed, John Wiley and Sons Inc, New York, (1977).
- Windet L. D., Pellegrini D., and Lee J., "**Coupled modeling of cement/claystone interactions and radionuclide migration**", *Journal of Contaminant Hydrology*, **68**, 165-182(2004).
- [www.quintessa.org](http://www.quintessa.org)
- [www.skb.se](http://www.skb.se)
- Xi J., He M., and Lin C., "**Adsorption of antimony(III) and antimony(V) on bentonite: kinetics, thermodynamics and anion competition**", *Microchemical Journal*, **97**(1), 85-91(2011).
- Xu D., Tan X.L., Chen C.L., and Wang X.K., "**Adsorption of Pb(II), from aqueous solution to MX-80 bentonite: effect of pH, ionic strength, foreign ions and temperature**", *Applied Clay Science*, **41**, 37-46(2008).
- Zahra N., Sheikh S. T., Mahmood A., and Javed K., "**Removal of arsenic from wastewater using bentonite**", *Bangladesh J. Sci. Ind. Res.*, **44**(1), 81-86(2009).

- Zavarin M., Powell B. A., Bourbin M., Zhao P., and Kersting A. B., "**Np(V) and Pu(V) ion exchange and surface-mediated reduction mechanisms on montmorillonite**", *Environ. Sci. Technol.*, **46**, 2692-2698(2012).
- Zavarin M., Kersting A. B., Begg J. D., Benedicto-Cordoba A., and Zaho P., "**Np(V) sorption and diffusion on montmorillonite clay progress report**", LLNL-TR-641530 report, (2013).
- Zhang L., Kanki T., Sano N., and Toyoda A., "**Development of TiO<sub>2</sub> photocatalyst reaction for water purification**", *Separation and Purification Technology*, **31**(1), 105-110(2003).
- Zhao G., Wu X., Tan X., and Wang X., "**Sorption of heavy metal ions from aqueous solutions: a review**", *The Open Colloid Science Journal*, **4**, 19-31(2011).

جامعة النجاح الوطنية  
كلية الدراسات العليا

# امتصاص الأيونات خماسية التكافؤ بواسطة طينة البنتونايت

إعداد  
سجود عدنان عودة

إشراف  
د. زيد نعيم قمحية  
د. خولة نعيم قمحية

قدمت هذه الأطروحة استكمالاً لمتطلبات الحصول على درجة الماجستير في الفيزياء بكلية الدراسات العليا في جامعة النجاح الوطنية في نابلس، فلسطين.

2015



ب

امتصاص الأيونات خماسية التكافؤ بواسطة طينة البنتونايت

إعداد

سجود عدنان عودة

إشراف

د. زيد نعيم قمحية

د. خولة نعيم قمحية

### الملخص

تناولت هذه الأطروحة دراسة عملية امتصاص المواد المشعة خماسية التكافؤ في طينة البنتونايت في نظامين من المحاليل الملحية مختلفة التركيز (المياه الجوفية وماء البحر). حيث تم استخدام محاكاة الجراندي كانونكال مونت كارلو (Grand canonical Monte Carlo simulation) وذلك بالاعتماد على النموذج البدائي (Primitive model). في هذا النموذج تم اعتبار أن المذيب (الماء) يمتلك ثابت النفاذية العازل (78) وأن الأيونات لها نفس القطر (4) انجستروم. خلال هذا العمل افترض بأن النظام ككل في وضع اتزان مع المحلول الملحي. وتم التحقق من العوامل المؤثرة في عملية الامتصاص من خلال حساب معدل تركيز الأيونات خماسية الشحنة في الطبقة الكهربائية المزدوجة (Average electrical double layer concentration) وأيضا من دراسة سلوك معامل الامتصاص لهذه الأيونات (Retention coefficient).

وبناء على نتائج هذه الدراسة تم التوصل الى أن معامل الامتصاص للأيونات خماسية التكافؤ يزداد بشكل ملحوظ بازدياد قيمة كثافة الشحنة على سطح صفيحة الطين. لكن في المقابل يتناقص معامل الامتصاص بازدياد تركيز المواد المشعة في المحلول ودرجة حرارة النظام وتركيز ايونات المحلول (الصوديوم والبوتاسيوم). اضافة الى ذلك تم التأكد من أن حفظ المواد النووية في طينة البنتونايت طريقة فعالة ومجدية لامتصاص ومنع انتقال الاشعاعات الى الطبيعة. فضرر هذه المواد

ت

النوية يعود الى عمرها النصفى الطويل وسميتها حتى لو كانت متواجدة في تراكيز قليلة جدا. أما بالنسبة لطريقة محاكاة المونتي كارلو فقد اثبت بأنها طريقة دقيقة وفعالة واقتصادية لدراسة احتباس المواد المشعة في البنتونايت.